이학박사학위논문

The interactive effect between ozone, sulfate aerosol, East Asia summer monsoon under present and future climate

현재와 미래 기후에서의 오존, 황산염, 동아시아 몬순의 상호작용

2016년 2월

서울대학교 대학원

지구환경과학부

김 민 중

Abstract

Changing climate and air quality are strongly connected each other. For example, ozone and aerosol concentrations are strongly influenced by wind and temperature changes. Those air pollutants also play an important role in climate as a short-lived climate forcer. However, the understanding of the interaction between the two is still very low. This dissertation is to address the uncertainties of the interactive effects between climate change and air pollutants focusing on three objectives: (1) The effect of aerosol on the East Asian summer monsoon, (2) Future ozone and oxidants change under the RCP scenarios, and (3) Relationship changes between the East Asian summer monsoon and ozone in surface air in the present and future climate. I first examine the effect of anthropogenic aerosol forcing on the East Asian summer monsoon (EASM) using a general circulation model. One control and two sensitivity model experiments were conducted in order to diagnose the separate roles played by sea surface temperature (SST) variations and anthropogenic sulfate aerosol forcing changes in East Asia. I find that the SST variation has been a major driver for the observed weakening of the EASM, whereas the effect of the anthropogenic aerosol forcing has been opposite and has slightly intensified the EASM over the recent decades. The reinforcement of the EASM results from radiative cooling by the sulfate aerosol forcing, which decelerates the jet stream around the jet's exit region.

Subsequently, the secondary circulation induced by such a change in the jet stream leads to the increase in precipitation around 18-23°N. This result indicates that the increase in anthropogenic emissions over East Asia may play a role in compensating for the weakening of the EASM caused by the SST forcing. I investigate the ozone air quality changes in 2050 caused by global changes in climate and anthropogenic emissions of ozone precursors using a global chemical transport model driven by meteorological fields from a general circulation model. My model results show that annual mean concentrations of surface ozone will be lower in 2050 relative to 2000 by -3.3, -3.7, and -4.2 ppbv under RCP6.0, RCP4.5, and RCP2.6, respectively. In contrast, the RCP8.5 projection results in a slight increase of 2.1 ppbv caused by a methane increase. The ozone reductions are driven primarily by decreases in NO_x emission, which dominate the climate penalty on ozone driven by temperature increases. I also estimate the effect of 21st century climate change on ozone air quality, assuming no changes in anthropogenic emissions of ozone precursors in the future. Temperature increase is found to result in ozone increases of up to 2.2 ppbv over land. Ozone over the oceans, however, is largely reduced with specific humidity increase, particularly in Northern Hemisphere, where the ozone concentration decreases by 0.8 ppbv. I also examine the effect of the EASM change on surface ozone concentrations over East Asia using the GEOS-Chem, which is driven by meteorological fields from the Community Earth System Model (CESM). I

conduct model simulations using the RCP8.5 scenario to estimate the effects of the EASM on ozone 2000 and 2050. My model results show that ozone concentrations are positively correlated with the EASM in Central China. On the other hand, an opposite relationship is found in downwind regions including Eastern China, Korea, and Japan owing to a cyclonic circulation associated with the EASM. However, the relationship between the ozone change and the EASM becomes opposite in 2050 compared to that of 2000. The 2000-2050 change in the relationship between the ozone and the EASM is mainly due to a EASM domain shift under the warming climate in 2050, indicating the conventional EASM index based on the present climate condition cannot be applied to the future climate. Therefore, a modified EASM index is applied to examine the relationship between the two. I find, however, a weaker correlation between ozone and the EASM change in the downwind region in 2050, which is associated with the weakening of cyclonic circulation associated with the EASM over East Asia in 2050. These results indicate that the ozone change owing to the inter-annual variation of the EASM may change under the global warming climate.

Keyword: Ozone, Sulfate aerosol, East Asian summer monsoon, Climate change, Chemical Transport Model (CTM)

Student Number: 2008-20393

Table of Contents

Lists of Figures

Lists of Tables

CHAPTER Ⅰ

INTRODUCTION

1.1 Background and motivation

Air quality change is a critical issues for human health. According to medical studies, particulate matter and ozone in ambient air can damage the lungs and respiratory system (Bernard et al., 2001). Air quality is essentially determined by emission strength and meteorology (Jacob and Winner, 2009). Shifts in the weather strongly influence ozone and particle matters (Fiore et al., 2012). Due to the strong correlation between meteorological conditions and air quality, a changing climate is anticipated to impact the concentrations of pollutants in the atmosphere. Atmospheric warming associated with climate change has the potential to increase ground-level ozone in land regions, which is due to an increase of biogenic Volatile Organic Compounds (VOCs). Ozone over the oceans, however, is reduced with specific humidity increase (Jacob and Winner, 2009). The impact of climate change on particulate matter is less certain, but research is underway to address these uncertainties (Fiore et al., 2012).

As air pollution can have harmful effects on human health and

ecosystems, it can also impact the climate. Troposphere ozone is a significant contributor to climate warming. The most recent study estimates that radiative forcing of tropospheric ozone is 0.34 W m^{-2} from ACCMIP multi-model studies (Conley et al., 2013; Lamarque et al., 2013; Stevenson et al., 2013). The value indicates that tropospheric ozone is the third most important greenhouse gas (IPCC, 2013).

Particle pollution can also have significant impacts on climate, both directly and indirectly (IPCC, 2013). The direct effects come from particles' ability to absorb and scatter light. Different types of particles have different impacts on climate: some are warm, and others are cool (Stevenson et al., 2013). Black carbon, a component of soot particles, contributes to global warming by absorbing sunlight, thereby heating the atmosphere (Ramanathan et al., 2008). When black carbon is deposited on snow and ice, melting accelerates. Particle pollution can also have significant indirect effects on climate. For example, particles can change the reflectivity of clouds and also indirectly influence cloud lifetime and precipitation (Albrecht, 1989; Twomey, 1977).

The changing climate and air quality are strongly connected. Our society urgently needs to understand the linkage between climate change and air quality. The impact of the interaction between climate change and air quality is very uncertain. Several modeling studies have focused on interactions between

climate change and air quality to reduce uncertainty. However, many uncertainties remain.

1.2 East Asian summer monsoon change due to sulfate aerosol

Monsoons play a key role in global mass and heat transport (Trenberth et al., 2000). In particular, the East Asian monsoon is one of the strongest monsoon systems due to the combination of thermal contrast between the largest Asian continent and the Pacific (Wang and Ding, 2006). It covers both subtropics and mid-latitudes, and its concentrated rain belts stretch for many thousands of kilometers and affect China, Japan, Korea, and the surrounding areas (Wang et al., 2001).

The previous study (*Wang et al*., 2004 and reference therein) suggested that the East Asian summer monsoon was mainly influenced by the sea surface temperature (SST) forcings including El Nino-Southern Oscillation (ENSO), the western Pacific SST and the surrounding oceans. However, recent studies have argued that the increased aerosol forcing could also change monsoon system over East Asia (Liu et al., 2009). Aerosols can affect cloud and precipitation through their direct and indirect effects. (Haywood and Boucher, 2000, Twomey,

1977, Albrecht, 1989). For example, a cooling induced by the presence of scattering aerosol may suppress a monsoon circulation and decrease precipitation over East Asia (Iwasaki et al., 1998, Huang et al., 2007). The rapid industrialization over East Asia has provided a favorable atmospheric condition susceptible to the aerosol forcing because of a dramatic increase of primary aerosol and aerosol precursor emissions over the past several decades (Ohara et al., 2007). Subsequently, the enhancement of aerosol concentration is able to modulate the atmospheric circulation by perturbing cloud and precipitation, resulting in the changes in the monsoon system over East Asia (Wang et al., 2009).

Recent modeling studies with more sophisticated physics, however, have drawn contentious conclusions regarding the impact of aerosols on the East Asian monsoon system. Guo et al. (2013) showed that the East Asian monsoon was not significantly changed as anthropogenic sulfate aerosol increased during boreal summer. In contrast, Jiang et al. (2013b) showed that sulfate aerosol was able to enhance the monsoonal circulation. These results indicate that the effects of aerosol on East Asia summer monsoon have large uncertainty. Therefore, it is still debatable whether aerosol frocings could strengthen or weaken the monsoon over East Asia (Kuhlmann and Quaas, 2010).

1.3 Future ozone and oxidants change under warming climate

Rapid global climate change is expected in the coming decades (IPCC, 2007), and it may lead to ozone air quality change by affecting future air pollution meteorology (Jacob and Winner, 2009). This air quality change could directly affect human health (Bernard et al., 2001) and also climate by perturbing the Earth's radiation budget (Cionni et al., 2011, Eyring et al., 2013). For example, tropospheric ozone is a primary air pollutant and the third most important greenhouse gas (IPCC, 2013). Therefore, an accurate estimate of air pollutant concentrations including tropospheric ozone under future climate is critical for assessing impacts on both human health and climate change.

However, quantitative estimation of future ozone concentrations is very challenging because of a couple of confounding factors. First, future anthropogenic emissions of ozone precursors are very uncertain. A number of future emission scenarios have been developed based on socioeconomic projections (Vuuren et al., 2007, Fujino et al., 2006, Smith and Wigley, 2006, Riahi et al., 2007), but it is difficult to evaluate these, which seriously limits the credibility of the future projections (Webster et al., 2002). Such projected emissions should be considered as providing only a range of foreseeable changes for the future.

Another factor is change in air pollution meteorology, which directly affects the formation, transport, and loss of ozone and also modifies ozone precursor emissions from natural sources. For example, higher temperatures in a warming climate may increase ozone concentrations in surface air over continent because of enhanced chemical production and increased biogenic emissions of isoprene (Lin et al., 2008, Nolte et al., 2008, Unger et al., 2006, Wu et al., 2008a, Wu et al., 2008b, Liu et al., 2013a, Rasmussen et al., 2012, Katragkou et al., 2011). In addition, natural NO_x (NO_x = NO + NO_2) emissions from soil and lightning vary depending on meteorological conditions and are generally expected to increase in a warming climate (Banerjee et al., 2014, Sohi et al., 2010). Dentener et al. (2006), however, suggested that humidity increases in a warming climate would reduce ozone concentrations in the Northern Hemisphere because of enhanced conversion of ozone to OH radical. This conversion plays an important role in determining oxidation capacity and affects the lifetime of other air pollutants. Change in cloud fraction is another important but highly uncertain factor for future ozone (Meleux et al., 2007).

1.4 Relationship changes between the East Asian summer monsoon and ozone in surface air in the present and future climate

EASM has a significant impact on not only precipitation and dynamic systems but also ozone air quality over East Asia (*He et al.*, 2008; *Yang et al.*, 2014; *Zhou et al.*, 2013). The studies based on observation have revealed that the summer minimum of surface ozone over East Asia was attributed to the incursion of a monsoon that transports oceanic air (*Pochanart et al.*, 2002; *Wang et al.*, 2006; *Yamaji et al.*, 2006; *Zbinden et al.*, 2006; *Zhou et al.*, 2013). The East Asia monsoon not only affects the seasonal patterns of surface ozone over this region, but also results in the lowest summertime transport of pollutants during the year from the Asian continent to Japan and other regions because of the weak Asian outflow and northwestward penetration of the maritime air mass (*Yamaji et al.*, 2006; *Zbinden et al.*, 2006).

Yang et al. (2014) quantified the impacts of the East Asian summer monsoon on interannual variations of June-July-August (JJA) surface-layer ozone concentrations using assimilated meteorological fields and GEOS-Chem chemical transport model. They showed that ozone concentration averaged over

all of China is found to correlate positively with the EASM index by a large correlation coefficient of +0.75, indicating that summertime ozone concentrations are lower (or higher) in weaker (or stronger) EASM years.

On the other hand, global monsoon precipitation is expected to increase over the Northern Hemisphere (*IPCC*, 2013; *Lee and Wang*, 2014), and EASM also expects to increase in future (*IPCC*, 2013; *Seo et al.*, 2013). The future EASM system change can have a significant impact on future ozone air quality over East Asia. Previous modeling studies of future ozone air quality mostly focus on emission change in future (*Butler et al.*, 2012; *Cionni et al.*, 2011; *Fiore et al.*, 2012; *IPCC*, 2013; *Kawase et al.*, 2011; *Szopa et al.*, 2013; *Young et al.*, 2013). Monsoon system change in a warming climate greatly influences the ozone air quality in future. The impact of the EASM change on future ozone should be investigated.

1.5 Objective of the thesis

The changing climate and air quality are strongly connected to each other. Climate change strongly influences ozone and particle matters. Air pollution can also impact the climate. However, understanding of the interaction between climate change and air pollutants is limited. This dissertation addresses

these uncertainties. For this purpose, I use 3-D chemical transport model and general circulation model to estimate the effects of interaction between climate change and air pollutants.

The thesis includes three scientific issues. The objectives of this study are:

1. to examine future air quality change by focusing primarily on ozone concentrations using the RCP scenarios and attempting to reduce the associated uncertainty of future ozone projection;

2. to estimate the effect of aerosol on the East Asian summer monsoon using long-term ensemble simulations using an atmospheric general circulation model;

3. to investigate the relationship changes between the East Asian summer monsoon and ozone in surface air in the present and future climate.

CHAPTER Ⅱ

EFFECT OF SULFATE AEROSOL FORCINGS ON THE EAST ASIAN SUMMER MONSOON

2.1 Objective

The previous studies suggested that the East Asian summer monsoon system is primarily influenced by sea surface temperature (SST) forcings including El Niño-Southern Oscillation (ENSO), the western Pacific SST, and those of the surrounding oceans (*Wang et al.*, 2004 and references therein). However, recent studies have argued that increased aerosol forcing can also change the monsoon system over East Asia (*Liu et al.*, 2009) by affecting clouds and precipitation through direct and indirect effects (*Albrecht*, 1989; *Haywood and Boucher*, 2000; *Twomey*, 1977). The rapid industrialization of Asia has caused dramatic increases of primary aerosol and aerosol precursor emissions over the past half century (*Smith et al.*, 2011). The enhancement in aerosol concentration induces atmospheric cooling and suppresses monsoon circulation, resulting in a weakening of monsoon strength with a decreased precipitation over

Asia over the past decades (*Kim et al.*, 2007; *Bollasina et al.*, 2011; *Cowan and Cai*, 2011; *Ganguly et al.*, 2012; *Bollasina et al.*, 2014).

Recent modeling studies with more sophisticated physics, however, have drawn contentious conclusions regarding the impact of aerosols on the East Asian monsoon system. *Guo et al.* (2013) showed that the strength of East Asian monsoon has weakened due to the sulfate aerosol forcing in the post monsoon season, although the strength of East Asian monsoon has not significantly changed at the 95% significance level during which anthropogenic sulfate aerosol has increased in boreal summer. *Jiang et al.* (2013) showed CAM5 simulations that sulfate aerosol plays a role in enhancing the monsoonal circulation and precipitation over the South China Sea and the western Pacific Ocean. *Bollasina et al.* (2013) found that aerosols are likely responsible for the observed earlier Indian monsoon onset, resulting in enhanced precipitation over most of India during June. Based on CMIP5 results, *Guo et al.* (2014) suggested that the aerosol indirect effects are likely related to the negative rainfall trend, whereas the direct radiative effect is associated with the increase in monsoon rainfall. *Turner and Annamalai* [2012] concluded that the South Asian precipitation during the 20th century can not be explained by atmospheric CO_2 concentration and global temperature increase because of the effects of aerosols. Therefore, aerosol clearly represents a major uncertainty for the monsoon

projections in the future climate. In this study, I focus on the effect of aerosol on the East Asian summer monsoon (EASM) using a long-term ensemble simulations using an atmospheric general circulation model (AGCM).

2.2 Data and Methodology

2.2.1 Reanalysis dataset and monsoon index

I use the reanalysis datasets and the climate model simulation to explore the contributions of anthropogenic aerosol forcings on the EASM. The National Centers for Environmental Prediction (NCEP)/Department of Energy (DOE) reanalysis II (RA2) datasets (*Kanamitsu et al.*, 2002) is analyzed and I also use the Global Precipitation Climatology Project (GPCP) monthly precipitation dataset version 2.2 for 1985-2010 (Adler et al., 2003). Many EASM indices based on atmospheric thermodynamics and dynamics, such as pressure, ocean-land temperature contrast, wind field, and precipitation has been widely used to quantify the monsoon extent and its variability over monsoon regions (Wang et al., 2009). In the present study, I use the definition of EASM index following Li

and Zeng (2002) using the NCEP DOE RA2 dataset, which is referred to as the observation. The EASM index is defined as

$$\mathrm{EASMI} = \frac{||\overline{\mathrm{V}}_W - \mathrm{V}_i||}{||\overline{\mathrm{V}}||} - 2$$

where $\overline{\mathrm{V}}_W$ and V_i are the climatological winter wind vector as the reference state and monthly wind vectors at a point, respectively, and $\overline{\mathrm{V}} = (\overline{\mathrm{V}}_W + \overline{\mathrm{V}}_S)/2$ is the climatological mean wind vector. Here $\overline{\mathrm{V}}_S$ is the climatological summer wind (for the Northern Hemisphere, taking $\overline{\mathrm{V}}_W = \overline{\mathrm{V}}_{Jan}$ and $\overline{\mathrm{V}}_S = \overline{\mathrm{V}}_{Jul}$). The norm ||A|| is defined as

$$||\mathrm{A}|| = \left(\iint_S |A|^2 \, dS \right)^{1/2}$$

where here S now denotes the domain of integration. According to *Li and Zeng* (2002), the domain of EASM Index is defined as 10 - 40°N, and 110 – 140°E. This monsoon index is also used in previous studies (Li and Zeng, 2003, Zhu et al., 2012, Nan and Li, 2003) and NOAA Climate Prediction Center (http://www.cpc.ncep.noaa.gov/products/Global_Monsoons/Asian_Monsoons/monsoon_index.shtml). There is an apparent negatively correlation between the EASM index and the rainfall variability in the middle and lower valley of the Yangtze River in China during the boreal summer (June-July-August, JJA),

indicating drought years over the valley are associated with the strong EASM and flood years with the weak EASM (Nan and Li, 2003).

2.2.2 Model simulations

I performed model simulations using the NCAR Community Atmosphere Model version 5 (CAM5) model coupled with the Community Land Surface Model version 4 (*Neale et al.*, 2012). The CAM5 model is based on the finite volume (FV) dynamical core at a 1.9°×2.5° horizontal resolution and with 30 vertical levels. For this study, the ocean and ice modules were not fully coupled, but were communicated to the atmosphere via an oceanic surface boundary condition, given as mid-month values of sea surface temperature, as well as sea ice fractions over the polar region. The sea surface temperature and the sea ice fractions are time series data constructed by concatenating and interpolating global HadISST data from the Met Office Hadley Center (*Rayner et al.*, 2003) to the FV core grids of the CAM5. For aerosol simulations, the CAM5 uses a three-mode version of the modal aerosol model (MAM3) (*Liu et al.*, 2012).

To examine the role of sulfate aerosol forcing in East Asia, I updated the Asian anthropogenic SO_2 emissions in the CAM5 with the gridded inventory for 2000 over the Asian domain (60°E–158°E and 13°S–54°N) (*Streets et al.*, 2003).

The Asian emission of SO_2 for the year 2000 was 18.9 Tg S y^{-1}. I applied the annual scale factors of the Regional Emission inventory in Asia (REAS) (*Ohara et al.*, 2007) for 1985-2010 to the *Streets et al.* [2003] emissions in order to impose interannual variations in the model. The emission of SO_2 had continuously increased until 2006 and then has slightly decreased in East Asia. The SO_2 emission in 2006 was 84% higher than that in 1985. While the SO_2 emissions in other regions are fixed following *Liu et al*. (2012), the aerosol concentration in other regions may not be constant because it can be transported from one region to the others. Because MAM3 module is fully coupled with cloud physics and radiation code, CAM5 accounts for both aerosol direct and indirect effects with Asian sulfate aerosol change over the recent decades (*Neale et al.*, 2012).

I conducted three sets of model experiments using the CAM5. The first set used the historical SST for 1985-2010 with the time-varying SO_2 emissions in East Asia, hereafter referred to as the control run. The second set used the historical SST without the East Asian SO_2 emissions, which will be referred to as the SST-run. Finally, the third set included the climatological SST with the time-varying SO_2 emissions in East Asia, which will be referred to as the SO_2-run. Each set of experiments was performed with four ensemble members, the average of which is presented in this study. In this study, I mainly focused on the

effect of sulfate aerosol on EASM because the concentration of sulfate aerosol has dramatically increased in East Asia during the past few decades relative to those of other aerosol species such as brown and black carbon aerosols (*Streets et al.*, 2003, *Li et al.,* 2013).

2.3 Result

I first compare the observed mean precipitation and low-level (850hPa) winds during JJA with the simulated values from the control run for 1985-2010 (Figs. 2.1 a, b). The GPCP precipitation is the highest around the Philippines and Northern Mariana Islands. The second peak is located around southern China, Japan, and Korea, and is associated with the Baiu/Meiyu/Changma front (*Wang et al.*, 2004). On the other hand, the observed wind shows clear cyclonic circulation over southern Asia and southern China along with the southwesterlies from the ocean onto the land and anticyclonic circulation over the western North Pacific.

The control run captures the general patterns of the observed mean precipitation and low-level winds during JJA. In particular, the model reproduced the observed precipitation band from southwestern China to the

Korean peninsula. However, considerable discrepancies still exist in the detailed structures between the control run and the observation (Fig. 2.1c), indicating the model inability of precipitation simulation, which are likely caused by my limited scientific understanding as well as simulation capability for sub-grid scale processes. The overall amount of precipitation and the strength of circulation simulated in the control run are smaller and weaker than those in the observations, respectively. In addition, the magnitude of the precipitation band from southwestern China to the Korea peninsula is smaller than that of observation and its position is shifted to the north in the control run (Fig. 2.1c). Such model biases are also found in most of the CMIP3 and CMIP5 model participants (*Sperber et al.*, 2013). In spite of this difference, the spatial pattern in the precipitation variability associated with the EASM index in the control run is not much influenced by such discrepancies compared to the observation (see Fig. 2.2). In addition, the pattern correlation in the mean precipitation structure between the observation and the control run is 0.61 with the 95% statistical significance. Note that it is also found that the pattern correlation coefficient of each member in the control run is similar to that of the ensemble mean (Fig. 2.3 and Table 2.1). Furthermore, the precipitations and winds fields in the SST-run and the SO_2-run are also comparable with the control run (Fig. 2.4).

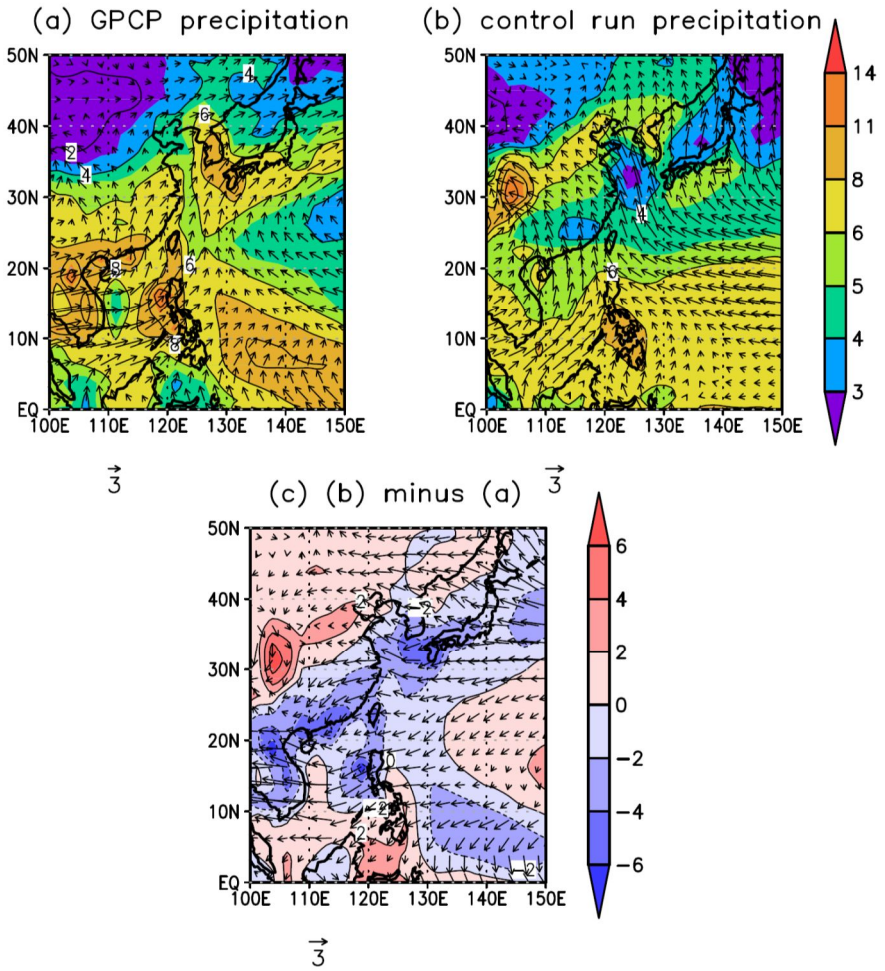

Fig. 2.1. (a) Boreal summer mean GPCP precipitation (shaded) and NCEP DOE RA2 wind fields at 850hPa (vector) for 1985-2010. (b) Same as (a) but for the CAM5 results (control run). (c) Difference between simulated and observed results. Unit in precipitation and wind is mm day^{-1}, and m s^{-1} respectively.

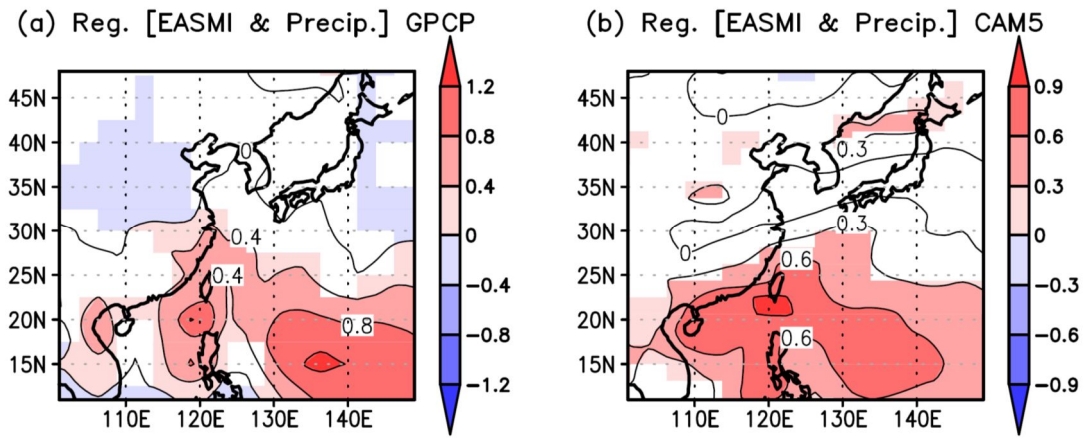

Fig. 2.2 (a) Regression of precipitation against the EASM index from the observation. Fig. S1b is the same as Fig. S1a except the control run. Unit is mm day^{-1}.Shaded denoted the statistical significance at the 95% confidence level.

Table 2.1. Pattern correlations between the precipitation of CAM5 and that of the GPCP.

	Set 1	Set 2	Set 3	Set 4	Ensemble
correlation	0.54	0.60	0.62	0.56	0.61

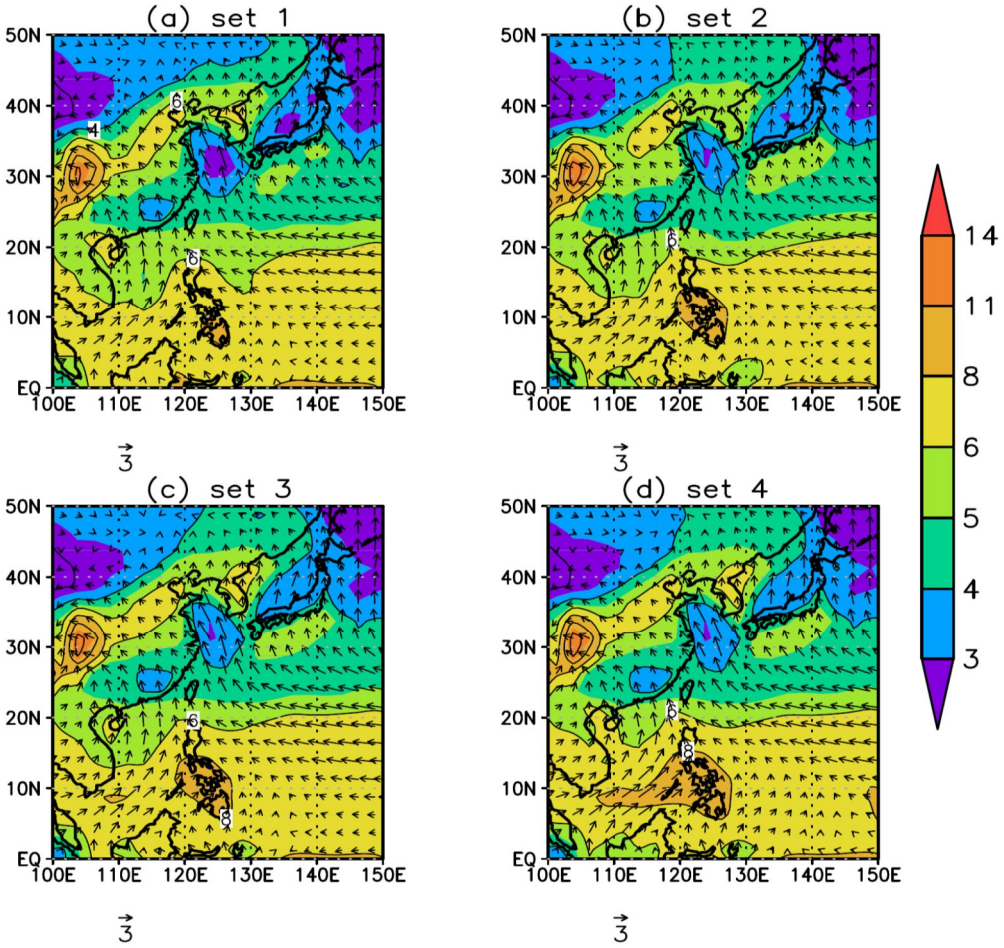

Fig. 2.3. Mean precipitation (shaded) and wind fields at 850hPa (vector) of each member in the control run for 1985-2010 during the boreal summer. Units are mm day^{-1}, and m s^{-1} respectively.

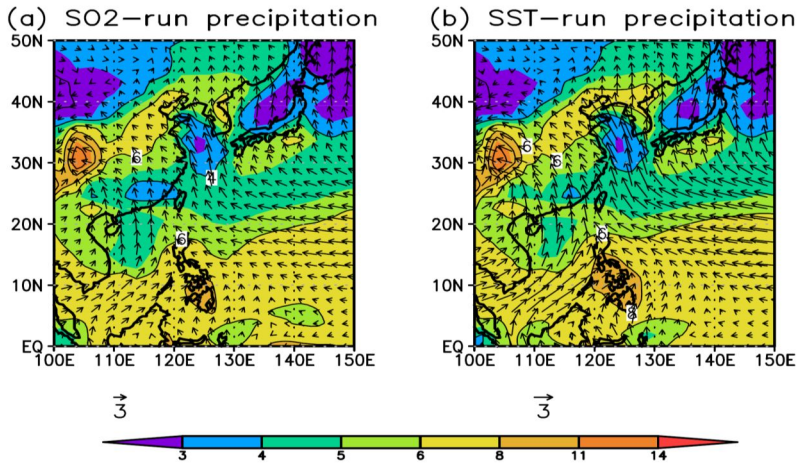

Fig. 2.4. (a) Mean precipitation (shaded) and wind fields at 850hPa (vector) simulated in the SO_2-run. Fig. S3b is the same as in Fig. S3a except the SST-run. Units are mm day^{-1}, and m s^{-1} respectively.

To examine the variability in the EASM, I calculate the EASM index in the observation, the control run, the SST-run, and the SO_2-run for 1985-2010 (Figs. 2.5a-d). Similar to many previous studies, the variability in the EASM is prominent on interannual timescales in the observation (*Shi and Zhu*, 1996; *Wang et al.*, 2008; *Zhu et al.*, 2005). In addition, it is evident that the EASM index is characterized by a slight decreasing trend in the observation (Fig. 2.5a). Such a weakening of the EASM is also found in both the control run and the SST-run (Figs. 2.5b, c), indicating that the overall variability in the EASM is reasonably simulated in the control run and the SST-run. It should be noted that

the decreasing trends in the control run and the SST-run are also statistically significant at the 95% confidence level. Therefore, the EASM index in the observation is highly correlated with those in the control run and the SST-run (see Table 2.1).

The EASM index simulated in the SO_2-run is characterized by a slightly increasing trend for 1985-2010, although the change is not statistically significant (Fig. 2.5d). This result is in contrast to the observations and the two other runs (control run and the SST-run), and it leads to negligible correlation coefficients of EASM indices between the SO_2-run and the others (Table 2.2). I argue that the contribution of sulfate aerosol trend acts to strengthen the EASM during recent decades, unlike SST forcing. In other words, the weakening of the EASM in recent decades is primarily due to SST forcing. A simple comparison of the trends of the EASM index in the three runs also supports this result. That is, the negative trend of the EASM index in the SST-run (-0.04 yr^{-1}) is slightly stronger than that of the control run (-0.03 yr^{-1}) owing to the effect of sulfate aerosol forcing, which strengthens the EASM in the control run. Therefore, the increase in sulfate aerosol concentration over East Asia lessens the negative trend of the EASM in the control run relative to that of the SST-run. It should be noted that when the first three years are removed, the observed trend of EASM becomes smaller (-0.002 $year^{-1}$ for 1988-2010) and the trend of EASM in each

member is comparable with the ensemble mean (Table 2.3). The simulated trends of the control-run, SST-run, and SO_2-run are also similarly reduced when the first three years are removed (-0.01 $year^{-1}$, -0.02 $year^{-1}$, and 0.01 $year^{-1}$) in the analysis. Despite of the smaller trends of the EASM both in the observation and simulations, however, the overall tendency does not change and is consistent with the results including the first three years.

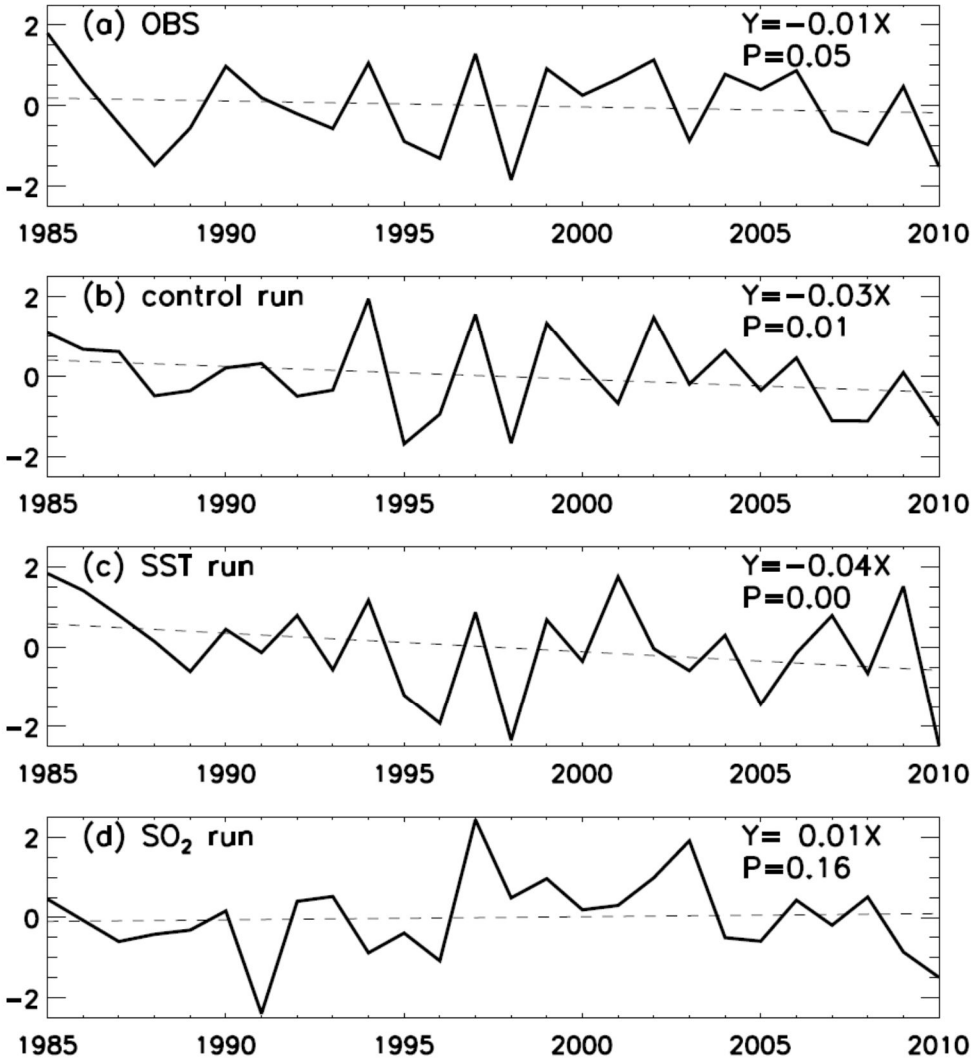

Fig. 2.5. Time-series of the EASM index from (a) the NCEP DOE RA2, (b) the control run, (c) the SST-run, and (d) the SO_2-run.

Table 2.2. Correlations between the EASM of the NCEP DOE RA2 and that of the control run, the SST-run, and the SO_2-run without the trend.

	Control run	SST-run	SO_2-run
NCEP DOE RA2	0.52	0.45	0.10
Control run	-	0.54	0.06

Table 2.3. significance level and trend of individual member in the control run, the SST-run, and the SO_2-run.

	Member 1		Member 2		Member 3		Member 4	
	Trend	P-Value	Trend	P-Value	Trend	P-Value	Trend	P-Value
Control run	-0.02	0.02	-0.05	0.01	-0.02	0.03	-0.04	0.01
SST run	-0.03	0.01	-0.03	0.01	-0.02	0.02	-0.09	0.00
SO_2 run	0.00	0.23	0.01	0.12	0.01	0.16	0.02	0.16

I investigate the opposite roles of the SST forcing and the sulfate aerosol forcing in modulating the intensity of the EASM by comparing the SST-run with the SO_2-run. I first calculate the regressed temperature against the EASM index in the SST-run (Fig. 2.6a). The regressed temperature at the upper troposphere is characterized by a warming (cooling) south (north) 40°N, which reflects an upper tropospheric condition during a strong EASM, as suggested by a previous study (*Yu et al.,* 2004). An enhancement of the meridional temperature gradient in East Asia leads to the northward shift of the jet stream, as shown in Fig. 2.6b. Subsequently, the northward shift of the jet stream drives the secondary circulation over East Asia, causing an increase in precipitation in East Asia (Fig. 2.6c).

In order to understand why the EASM becomes weaker in recent decades in the SST-run, I examine the differences in temperature and zonal wind at 300 hPa between 2001-2010 and 1985-1994 (2001-2010 minus 1985-1994) in the SST-run. I found that the meridional temperature gradient had weakened for 2001-2010 (Fig. 2.6d). As a result, the southward shift of the jet stream had occurred from 1985-1994 to 2001-2010, causing a decrease in precipitation in East Asia (Fig. 2.6e). This result implies that the observed weakening of the EASM is primarily explained by SST forcing. It should be noted that similar dynamic processes are found in the control run (not shown). In addition, the

regressed temperature, wind, and precipitation against the EASM index in the SO_2-run are displayed in the supplementary information (Fig. 2.7). It is found that the overall structures in the regressed temperature, wind, and precipitation against with the EASM index are similar to that in the SST-run, reflecting that the dynamical processes associated with a strong EASM are the same in the SST-run and the SO_2-run, respectively.

To estimate the effects of sulfate aerosol forcing in the SO_2-run for recent decades, the change in tropospheric temperature between the two periods (2001-2010 minus 1985-1994) in the SO_2-run is displayed in Fig. 2.8a. The increase of sulfate aerosol concentrations causes cooling in southeastern China, reflecting the thermal response due to either direct or indirect forcings of sulfate aerosol. I find, however, the simulated changes of cloud fraction and cloud radiative forcing in the SO_2-run are relatively small between the two periods (Figs. 2.9 in the supplementary information), indicating that the simulated indirect forcing owing to the sulfate aerosol change plays a minor role in modulating the thermal response in the model. In this work, I did not separate the direct and indirect effects of sulfate aerosols on the EASM. However, explicit understanding of each aerosol effect is critical to include the roles of aerosols in climate variability in global models. I plan to address this issue with improved models in the near future.

However, the changes of cloud fraction and cloud radiative forcing, which are closely associated with an indirect forcing, are small between the two periods in the SO_2-run (Figs. 2.9 in the supplementary information), indicating that the cooling in southeastern China is mainly due to a direct forcing. I can not quantitatively divide a direct or an indirect forcing because the NCAR CAM5 has a fully interactive chemistry module. However, estimation of the quantitative contribution between direct and indirect forcings of aerosol should be explored to examine the effects of aerosol forcing on the EASM with global climate modeling studies.

Strong cooling at 25°N-35°N in the low troposphere acts to change the meridional temperature gradient in eastern China. Concurrently, a weakening in the temperature gradient in eastern China results in a decelerating jet stream, as shown in Fig. 2.8b, which displays the differences in zonal and meridional circulation averaged over the 100°E-140°E between the two periods in the SO_2-run. My analysis of the results from the SO_2-run reveals that the radiative cooling owing to the enhancement of sulfate aerosol decelerates the upper level jet stream at the jet exit region, as indicated by the negative upper level zonal wind anomaly at 35–45°N. This jet weakening induces secondary circulation with rising motion around 18-23°N and sinking motion around 35-40°N and

causes an increase in precipitation around 18-23°N, resulting in a slight increase of EASM intensity (Fig. 2.8c).

According to the previous study (*Jacobson and Kaufman,* 2006), aerosols forcing can cause the SST cooling with the reduction of wind speeds by stabilizing air, which is consistent with a reduction in wind speed over land in China (Fig. 2.8b). Subsequently, a reduction of wind speed is able to cause less water evaporation over the ocean, contributing to the weakening of the EASM (*Jacobson and Kaufman,* 2006). The SO_2-run does not consider the feedback process between sulfate aerosol forcing and SST, therefore, I can not exclude the possibility that the intensity of EASM in the SO_2-run would be changed by allowing SST-ocean interactions. However, it is found that the difference in 2m-air temperature between the two periods (2001-2010 minus 1985-1994) in the SO_2-run is small over the ocean (Fig. 2.10 in the supplementary information). This indicates that the effect of SST changes due to sulfate aerosol forcing might be small, which may be due to a very short lifetime of sulfate aerosol in ambient atmosphere around 3~5 days (*Park et al.,* 2004).

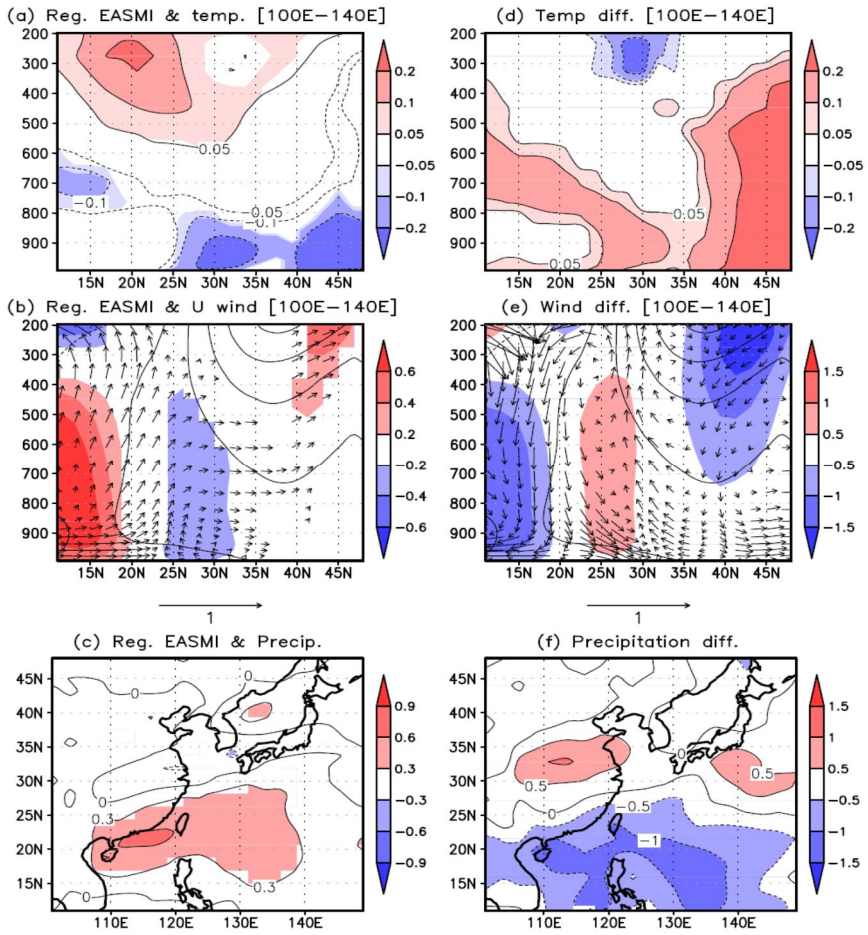

Fig. 2.6. (a) Zonally-averaged regression of temperature against the EASM index from the SST-run (100°E-140°E). (b) Zonally-averaged regression of wind field against the EASM index (shade = zonal wind, vector = v; omega × -30). The solid line indicates the averaged zonal wind (1985-2010, contour interval = 5). (c) Regression of precipitation against the EASM index. Shaded denoted the statistical significance at the 95% confidence level. The differences in (d) zonally-averaged temperature, (e) zonally-averaged wind, and (f) precipitation between the two periods (2001-2010 minus 1985-1994) in the SST-run. Units are K, m s^{-1}, mm day^{-1}, K, m s^{-1}, and mm day^{-1} respectively.

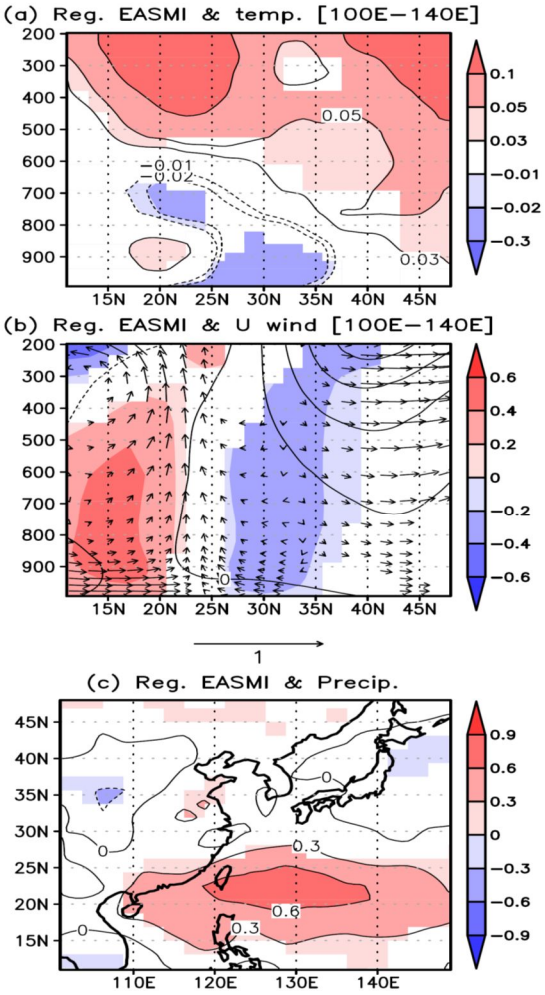

Fig. 2.7. (a) Zonally-averaged regression of temperature against the EASM index from the SO_2-run (100°E-140°E). (b) Zonally-averaged regression of wind field against the EASM index (shade = zonal wind, vector = v; omega × -30). The solid line indicates the averaged zonal wind (1985-2010, contour interval = 5). (c) Regression of precipitation against the EASM index. Units are K, m s^{-1}, mm day^{-1}, K, m s^{-1}, and mm day^{-1} respectively. Shaded denoted the statistical significance at the 95% confidence level.

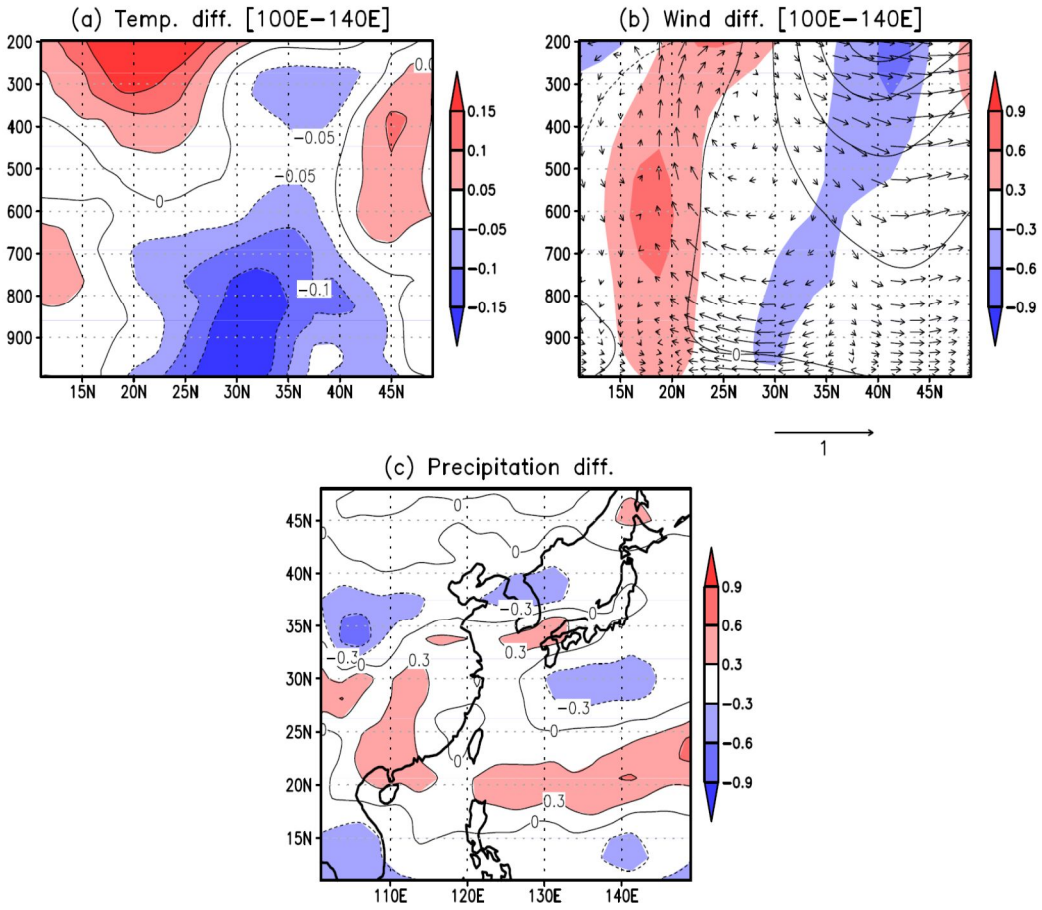

Fig. 2.8. Differences in (a) temperature averaged over 100°E-140°E, (b) zonal wind (shading) and meridional circulation (vector = v; omega × -30) averaged over 100°E-140°E, and (c) surface precipitation between the two periods (2001-2010 minus 1985-1994) in the SO_2-run. Units are K, K, m s^{-1}, and mm day^{-1}, respectively. The solid line in (b) indicates the averaged zonal wind (1985-2010, contour interval = 5).

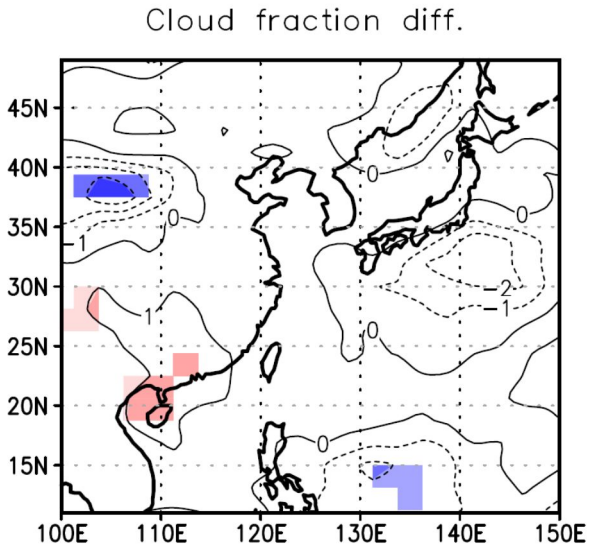

Fig. 2.9. Total cloud fraction difference between two periods (2001-2010 minus 1985-1994) in the SO_2-run. Shaded denoted the statistical significance at the 95% confidence level.

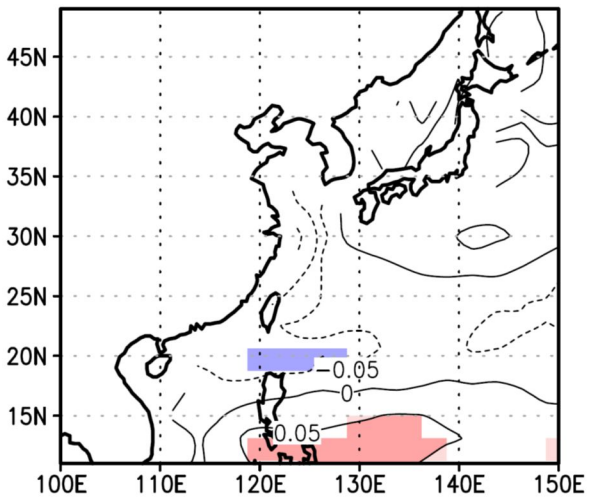

Fig. 2.10. The differences of 2m-air temperature between the two periods (2001-2010 minus 1985-1994) in the SO_2-run. Shaded denotes the statistical significance at the 95% confidence level.

3.4 Summary

To examine the effects of sulfate aerosol forcing on the EASM, I conducted three sets of CAM5 model experiments including control run, SST-run, and SO_2-run. Each set of experiments was performed with four ensemble members, the average of which was compared with the observations. The model reasonably captured the general patterns of precipitation and low-level winds over East Asia during JJA, although it failed to reproduce the detailed precipitation structures, reflecting the deficiency of the present global models.

My analysis of the EASM index based on the observations showed that the intensity of the EASM has decreased over the past few decades, which is consistent with the previous studies (*Yu et al.,* 2004; *Wang et al.*, 2009). I found that both the control run and the SST-run reproduced such a weakening of the EASM. In contrast, the model with anthropogenic sulfate forcing showed a slight increasing trend of the EASM index, indicating that SST forcing has resulted in the weakening of the EASM, while the effect of regional sulfate aerosol forcing acts to strengthen the EASM for 1985-2010. The weakening of the EASM due to SST forcigns is mainly associated with the weakening of meridional temperature gradient for 2001-2010 along with the southward shift of the jet stream. This

results in a downward motion at the right exit of the jet, causing a decrease in precipitation around 20^{O}N. On the other hand, the effect of sulfate aerosol forcing causes a cooling in southeastern China, which results in the weakening of the meridional temperature gradient in eastern China. As a result, the upper level jet stream decelerates at the jet exit region with the rising motion in southeastern. Consequently, an increase in precipitation around 18-23°N is induced by the effect of sulfate aerosol forcing over East Asia.

CHAPTER Ⅲ

FUTURE OZONE AND OXIDANTS CHANGE UNDER THE RCP SCENARIOS

3.1 Objective

Previous studies have used a coupled general circulation model–chemical transport model (GCM–CTM) approach to examine the effect of climate change on future ozone air quality based on the Intergovernmental Panel on Climate Change (IPCC) Special Report on Emissions Scenarios (SRES) and the recently released Representative Concentration Pathways (RCP) emission scenarios, which are developed for The Coupled Model Intercomparison Project phase 5 modeling (Taylor et al., 2012) and have attempted to understand the roles of individual processes affecting future ozone air quality. The simulated future ozone concentrations differ substantially depending on the SRES and RCP scenarios. The first results in a general increase (Dentener et al., 2006, Zeng et al., 2008, Fiore et al., 2012, Brasseur et al., 2006), but the latter is the opposite (Kawase et al., 2011, Cionni et al., 2011, Butler et al., 2012, Szopa et al., 2013, Fiore et al., 2012, IPCC, 2013, Young et al., 2013). The discrepancy is associated

primarily with the projection of changes in ozone precursors, for which the RCP scenarios generally assume significant future reductions. This contrasting outcome indicates the high uncertainty of future ozone air quality estimates and emphasizes the need for intensive studies focusing on process-level understandings of how ozone concentrations are affected by changes in precursors and meteorological conditions.

Here, I examine future air quality change by focusing primarily on ozone concentrations using the RCP scenarios and attempt to reduce the associated uncertainty of future ozone projection. For this purpose, I updated a global 3-D chemical transport model (GEOS-Chem) (Bey et al., 2001) to be driven by meteorological fields from the National Center for Atmospheric Research (NCAR) Community Earth System Model (CESM), which is an updated version of the model used by Vertenstein et al. (2012). I also present efficient statistical techniques to quantify the effect of change in each meteorological variable on future ozone concentrations. I first evaluate the performance of my modeling system by comparing simulated versus observed past ozone concentrations. I then conduct model simulations for 2050 using all four RCP scenarios (RCP2.6, RCP4.5, RCP6.0, and RCP8.5) to estimate future ozone air quality. I also use statistical analysis along with a few sensitivity simulations to investigate the effects of climate changes on ozone air quality and

other reactive gases, particularly under the RCP8.5 scenario.

3.2 Methods

3.2.1 Development of GEOS-Chem and CESM linking

GEOS-Chem has been driven by the NASA/Goddard Earth Observing System (GEOS) assimilated meteorology. Wu et al. (2007) first presented a linking system of GEOS-Chem with the Goddard Institute for Space Studies (GISS) GCM 3 to investigate the effects of SRES A1B 2000–2050 global change on ozone air quality in the United States (Wu et al., 2008b). This modeling system has been applied in previous studies for future tropospheric ozone and background surface ozone concentration changes in the United States (Wu et al., 2008a), future sulfate, nitrate, and ammonium aerosol changes in the United States (Pye et al., 2009), future aerosol trends and their radiative forcing (Leibensperger et al., 2012), and ozone changes in China (Wang et al., 2013). I generally follow the approach of Wu et al. (2007), with a few differences discussed below.

I use GEOS-Chem version 8-01-03, which includes a fully coupled treatment of tropospheric O_3–NO_x–VOCs chemistry and aerosols (Park et al.,

2004). I updated the isoprene oxidation mechanism for HNO_3 production (Mao et al., 2013). This update results in a decrease of isoprene nitrate yield (from 18% to 11.7%) and partial recycling of NO_x. Cross-tropopause ozone flux is computed with the Synoz parameterization (McLinden et al., 2000) with an imposed global annual mean flux of 480–490 Tg yr^{-1} (this variability reflects year-to-year differences in the model circulation). The stratospheric influxes of NO_x and total reactive nitrogen oxides (NO_y) are 0.4 and 2.4–2.5 Tg yr^{-1}, respectively.

I modified GEOS-Chem to use meteorology from the CESM climate model that employs an advection scheme identical to that of Lin and Rood (1996) so that it is straightforward for GEOS-Chem to use the simulated dynamical variables, such as winds and temperatures, from CESM. However, the wet convection schemes in GEOS-Chem differ in different GEOS versions; GEOS-3 and GEOS-5 use the Relaxed Arakawa–Schubert convection scheme (Moorthi and Suarez, 1992), whereas GEOS-4 has separate treatments of deep and shallow convection with the schemes of Zhang and McFarlane (1995) and Hack (1994). CESM uses the Zhang and McFarlane (1995) scheme for deep convection, which is consistent with that of GEOS-4, but does not include the Hack shallow convection. The absence of shallow convection scheme in this study likely results in weakening of vertical mixing especially in regions of active shallow convention such as northeastern Pacific (de Szoeke et al., 2006). I think that this

difference would have a small impact on ozone because of relatively low ozone concentrations over the ocean. However, species emitted from the ocean could be significantly affected, and thus the effect of the different treatment of convective mixing will be further examined in a future study. The treatment of boundary layer turbulence in CESM is the same as that in GEOS-Chem. The mixing depth in GEOS and CESM is estimated from the bulk Richardson number with surface friction (Holtslag and Boville, 1993).

I use CESM version 1.0.4. The model consists of Community Atmosphere Model 4 for the atmosphere and Community Land Model 4 with Carbon Nitrogen model for land. Parallel Ocean Program 3 and Community Ice Sheet Model 2 are used for ocean and sea ice calculation, respectively. Gent et al. (2011) described a spin-up procedure for the model. I performed an 1850–2006 historical simulation with the long-lived greenhouse gases emissions described in Gent et al. (2011). I conducted climate simulations for 2006–2100 using the RCP2.6, RCP4.5, RCP6.0, and RCP8.5 emission scenarios, considering primarily the changes in long-lived greenhouse gases (though the CESM simulations begin in 2005 to provide overlap with the historical and future forcings for a smooth transition in 2006). The model configuration generally follows that of Meehl et al. (2012).

Meteorological outputs from the CESM simulations were archived with

6-h resolution (3-h for surface quantities and mixing depths) for input to GEOS-Chem, which is consistent with the NASA GEOS assimilated meteorology (Bey et al., 2001). The output of CESM has a horizontal resolution of 0.9° x 1.25° and 26 sigma levels in the vertical extending from the surface to 2.6 hPa (~39 km altitude). I degrade the horizontal resolution to 2.0° x 2.5° to increase the computational efficiency of GEOS-Chem simulations. To account for interannual variability, the GEOS-Chem simulations are conducted for 10 years, 1996–2005 for the present-day climate (2000) under historical simulation and 2046–2055 for the future climate (2050) under each RCP scenario.

I use the emissions compiled by Choi et al. (2014), who calculated 1995–2055 anthropogenic (including ship and aircraft) and biomass-burning emissions of ozone precursors based on the reference data of RCP emissions (RCP database online at http://tntcat.iiasa.ac.at:8787/ RcpDb/dsd?Action=htmlpage&page=compare). My global emissions have similar magnitude to the reference data, but differ in a few ways. First, the reference RCP emissions are provided only every 10 years; therefore, I use a linear interpolation of decadal values to compile the annual trajectory of emissions for each year. I also detail emission sectors of RCPs' volatile organic compounds following the EDGAR 3.2 FT 2000 inventory (Olivier et al., 2005). I speciate total VOC emissions from each source according to the SAPRC99 chemical mechanism by using the US

EPA speciation profile and a source mapping method between the EDGAR and the US national emission inventory (Woo et al., 2012). Finally, I reclassify the VOC species of the SAPRC99 mechanism to GEOS-Chem species following Moon et al. (2004). Mixing ratios of methane for each simulated year in each RCP scenario are fixed throughout the entire model domain at the recommended values from IPCC AR5 report (IPCC, 2013). My emissions and background methane concentrations for the present and for 2050 are summarized in Table 3.1. Ozone precursor emissions of this study are comparable to those of previous RCP modeling studies (Szopa et al., 2013, Butler et al., 2012, Kawase et al., 2011).

Lightning and biogenic emissions are computed locally within the model. Lightning NO_x emissions are parameterized as a function of deep convective cloud top (Li et al., 2005) and are distributed vertically following Pickering et al. (1998). Simulated lightning NO_x emissions in the model are 5.0 Tg N yr^{-1} for the 2000 climate and 5.7 Tg N yr^{-1} for 2050 under the RCP8.5 scenario, and these are 3% and 6% less than the global emissions in other RCP model runs reported by Kawase et al. (2011), reflecting differences in the lighting parameterization and the driving meteorology. Soil NO_x emissions are calculated as a function of vegetation type, temperature, precipitation, fertilizer usage, and leaf area index following Wang et al. (1998). For biogenic VOC (BVOC)

emissions, I use the Model of Emissions of Gases and Aerosols from Nature (MEGAN) inventory (Guenther et al., 2006). Biomass burning emissions are projected according to the reference data of RCP emissions (Choi et al., 2014).

Table 3.1. Global Emissions of O_3 Precursors in simulation. Fixed emission used evaluation of model and sensitivity simulation.

	RCP scenario simulation					Fixed emission simulation
	Present day	2050s RCR 2.6	2050s RCR 4.5	2050s RCP 6.0	2050s RCP 8.5	
Anthropogenic NO_x, Tg N yr^{-1}	33.0	23.6	24.6	30.1	32.1	25.8
Lightning NO_x, Tg N yr^{-1}	5.0	5.3	5.3	5.5	5.7	-
Soil NO_x, Tg N yr^{-1}	6.7	7.0	7.1	7.2	7.3	-
Biomass NOx, Tg N yr^{-1}	5.4	4.9	4.2	5.7	5.0	6.5
Anthropogenic CO, Tg CO yr^{-1}	1068	820	872	1034	906	1034
Biomass CO , Tg CO yr^{-1}	459	414	307	482	398	459
Anthropogenic VOC, Tg C yr^{-1}	41.7	33.5	36.7	43.5	42.5	43.2
Biogenic VOC, Tg C yr^{-1}	632	686	691	719	771	-
Biomass VOC, Tg C yr^{-1}	10.3	9.1	6.7	11.0	8.9	10.1

3.2.2 Statistical method

Ozone production and loss vary sensitively with the change in each meteorological variable. The effects of meteorological variables on ozone are complex because they typically occur simultaneously and are interrelated. The quantification of each meteorological effect on ozone is computationally expensive because I need to conduct as many simulations as variables by changing the variable of interest while keeping the others the same. Statistical methods are fast and cheap and have been applied successfully to diagnose the effects of past climate change on air quality (Tai et al., 2010, Tai et al., 2012b, Tai et al., 2012a), although these have inherent uncertainties from the statistical error caused by random fluctuations or natural variability within the system.

To quantify the contributions of changes in individual meteorological variables to ozone concentrations, I use a multiple linear regression method. The selection of meteorological variables that serve as predictors for ozone (predictands) is important for this analysis. I first use partial correlation analysis to select predictor variables having partial correlation coefficients with ozone that are higher than 0.2. The selected variables construct a multiple linear regression model as follows:

$$y(t)-\bar{y} = \beta_0 + \beta_1(x_1-\bar{x}_1) + \beta_2(x_2-\bar{x}_2) + \ldots + \beta_n(x_n-\bar{x}_n) + \ldots + \varepsilon, \qquad (3.1)$$

where y and $\bar{y}$ represent the deseasonalized daily surface ozone concentration and time-averaged surface ozone concentration and x_k represents the deseasonalized meteorological variables from CESM. $\bar{x}_k$ is the seasonal mean of each meteorological variable, and β_k is the multiple regression coefficient, reflecting the explained variance of predictand by predictor. ε is noise from random fluctuations or natural variability within the system. All data (x_k and y) are deseasonalized and detrended by subtracting the 30-day moving averages from the original data. This allows us to focus on synoptic-scale variability and to avoid aliasing from common seasonal or interannual variations.

The multiple linear regression model has a critical weakness, especially when applying it to meteorological variables that are correlated to some degree. It is significant only if predictor variables are independent of each other. I use the Gram–Schmidt orthonormalization to overcome this weakness by constructing a set of orthonormal basis functions (Werneth et al., 2010), as shown in equation (3.2). x'_k indicates the orthonormalized meteorological variable by the Gram–Schmidt method. $proj_{x'k \bullet xj}$ represents the inner product of x'_k and x_j.

$$x'_1 = \frac{x_1}{|x_1|}$$

$$x'_2 = \frac{x_2}{|x_2|} - proj_{x'1 \bullet x2} \frac{x_2}{|x_2|} \cdot x'_1$$

$$x'_3 = \frac{x_3}{|x_3|} - proj_{x'1 \bullet x3} \frac{x_3}{|x_3|} \cdot x'_1 - proj_{x'2 \bullet x3} \frac{x_3}{|x_3|} \cdot x'_2 \qquad (3.2)$$

.

.

I use time series data. Therefore, the Gram–Schmidt orthonormalization should be rewritten as equation (3.3).

$$x'_1 = \frac{x_1}{|x_1|}$$

$$x'_2 = \frac{x_2}{|x_2|} - cov_{x'1 \bullet x2} \frac{x_2}{|x_2|} \cdot x'_1$$

$$x'_3 = \frac{x_3}{|x_3|} - cov_{x'1 \bullet x3} \frac{x_3}{|x_3|} \cdot x'_1 - cov_{x'2 \bullet x3} \frac{x_3}{|x_3|} \cdot x'_2 \qquad (3.3)$$

.

.

The regression equation with the n orthonormalized variables can be rewritten as follows:

$$y(t) - \bar{y} = X_o + X_1 + X_2 + \ldots + X_n + \varepsilon, \qquad (3.4)$$

where $X_k = \beta'_k(x'_k - \bar{x}'_k)$ and X_o is the intercept of the equation. I construct the

multiple linear regression models for the simulated ozone of each grid cell. Each term (X_k) represents the ozone changes corresponding to the variation of each orthonormalized meteorological variable. The order of each variable is important for the Gram–Schmidt orthonormalization, which statistically removes covariance between variables. Therefore, the first variable includes covariance with the others and the last variable includes only the independent component from the others. I examine the sensitivity of my analysis to the order of meteorological variables later, and I also calculate the covariance effect between two variables on ozone by switching the first and second order.

3.3 Model evaluation

Previous ozone evaluations of GEOS-Chem have been done extensively by a number of studies by comparing the model with surface, ozone sonde, satellite, and aircraft observations in North America, Europe, and East Asia (Kim et al., 2013, Alvarado et al., 2010, Jeong and Park, 2013). In this section, I evaluate the model driven by meteorology from CESM by focusing on the observed climatological features of ozone concentrations because the results from free-running GCM simulations do not represent the meteorological conditions for the specific year of simulation (Logan, 1999).

I first conduct GEOS-Chem simulations for 1999–2001 with the default emissions that consist of national emission inventories for anthropogenic species, including the European Monitoring and Evaluation Program (EMEP) inventory for Europe, the U.S. Environmental Protection Agency 1999 National Emissions Inventory for the U.S., the Streets et al. (2003) inventory for Asia, and the global emissions from the Global Emission Inventory Activity (GEIA) otherwise, scaled to the simulation years. Annual emissions of ozone precursors are summarized in Table 3.1.

For the model evaluation, I use ozone sonde profile measurements for 1996–2006 from the World Ozone and Ultraviolet Radiation Data Centre (WOUDC, http://www.woudc.org). The majority of the measurements were made in Europe and North America, but some were taken at a few stations in South America, Asia, and Africa. The WOUDC ozone profiles were measured by electrochemical concentration cell (ECC) (Komhyr, 1969) and Brewer Mast (BM) sondes. Recent comparisons between ECC and BM sonde measurements showed a level of agreement to within 5% and indicated that the observed differences between the two sonde types are not significant at the 90% confidence level (Stubi and Levrat, 2008).

Figure 3.1 compares the simulated and observed seasonal mean ozone concentrations in surface air at the WOUDC sites for the present day. The

observations show a clear seasonal variation such that values over the Northern Hemisphere are highest in JJA and lowest in DJF. High ozone concentrations appear in industrialized regions such as eastern North America, Europe, and Asia. In MAM, the highest ozone concentrations over the Himalayas are due to downward transport of stratospheric ozone (Kazimirovsky and Matafonov, 1998). The monsoonal circulations have a clear impact on the observed ozone concentrations in India and East Asia, where values in JJA are lower than those in MAM. The simulated ozone concentrations in surface air show seasonal and spatial patterns similar to those of the observations.

Figure 3.2 compares the observed and simulated monthly mean concentrations at 800, 500, and 300 hPa at the selected WOUDC ozone sonde sites. The observations show a general increasing trend with altitude owing to stratospheric influence (note the different scales of the y-axis) and the broad midyear maximum in the Northern Hemisphere (Legionowo, Egbert, and Madrid). Peaks occur over the polluted continents (Legionowo in Poland, Madrid in Spain, and Egbert in Canada) in summer, whereas the spring maximum occurs at remote sites such as Kagosima in Japan and Suva in Fiji. The effect of the Asian summer monsoon is shown clearly at the Kagoshima site (ozone decreases in summer at 800 hPa) (Gettelman et al., 2004).

Figure 3.2 also shows the two simulated results for comparison. The one

in blue is from GEOS-Chem driven by the CESM meteorology (1999-2001), and the other in red is from GEOS-Chem driven by the GEOS-4 assimilated meteorology for 1996-2006 (Bey et al., 2001). Both models generally capture the observed features, such as the broad summer maximum at 800 and 500 hPa at Legionowo, Madrid, and Egbert and the spring maximum at Kagosima and Suva. They also successfully reproduce the summer ozone decrease at Kagoshima driven by the monsoonal circulation. However, the results from GEOS-Chem/CESM are slightly higher than the observations and those of GEOS-Chem/GEOS4, especially in the low and mid-troposphere at Madrid and Egbert in summer and fall. The Atmospheric Chemistry and Climate Model Intercomparison Project (ACCMIP) (Lamarque et al., 2013b) showed that the majority of the models have a positive bias of ozone in the NH extratropics in the low and mid-troposphere, likely caused by errors in the VOC emissions (Young et al., 2013). My model also has a 14% positive bias of ozone in the NH extratropics, which is comparable to the 13% positive bias of the ACCMIP multi-model mean. The model, however, does not have a significant bias in the SH tropics, where the ACCMIC multi-model mean showed a 9% negative bias of ozone.

Figure 3.3 shows scatter plot comparisons of the observed versus simulated monthly mean concentrations of ozone at 800, 500, and 300 hPa at all

ozone sonde sites. The coefficients of determination between the observations and GEOS-Chem/CESM at 800, 500, and 300 hPa are 0.7 or higher, and these are comparable with those of GEOS-Chem/GEOS-4. The regression slopes between the observed and simulated values are close to unity, indicating no significant biases in the models, except at 300 hPa where GEOS-Chem/CESM shows a lower regression slope (0.7) relative to the result by GEOS-4. This low bias is due to the coarse vertical resolution of CESM, especially around the tropopause altitude. The model could not capture episodic increases in ozone concentration caused by tropopause folding events (Shapiro, 1980). Nevertheless, the bias does not appear to affect ozone concentrations significantly in the lower troposphere or especially at the surface, which is the primary focus of my analysis below.

I also compared my tropospheric ozone burden from GEOS-Chem/CESM with the ACCMIP results. My total tropospheric ozone burden is 321 Tg, which is 5% lower than the multi model mean of 337 Tg, but the value is within the range of multi-model estimates (Young et al., 2013). Tropospheric ozone burdens as a function of height and latitude are also summarized in Table 3.2 for a comparison with Fig. 2 of Young et al. (2013) and they are also within the range of the ACCMIP estimates, indicating that my model generally captures the distribution of the mean ozone burden throughout the troposphere to a degree

of other global models and is also successful for capturing the climatological features of the present-day ozone concentrations.

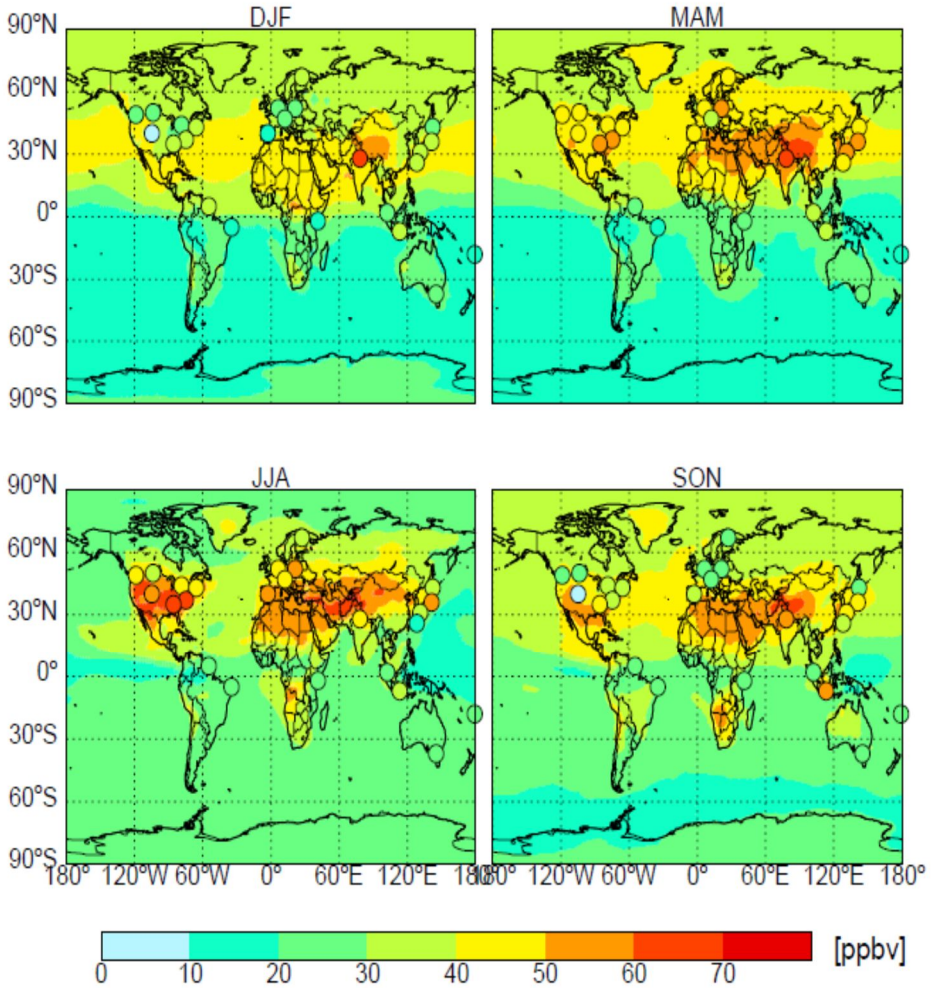

Fig 3.1. Surface ozone concentration from GEOS-Chem driven by CESM meteorological at 1999~2001. Circles indicate observed surface ozone from WOUDC ozonesonde data (1996~ 2005). Figure 1. Comparisons of the simulated and observed seasonal mean concentrations of ozone in surface air. The simulated values are from GEOS-Chem simulations driven by the CESM meteorology for 1999–2001. Closed circles indicate observations averaged for 1996–2005 at WOUDC ozone sonde sites.

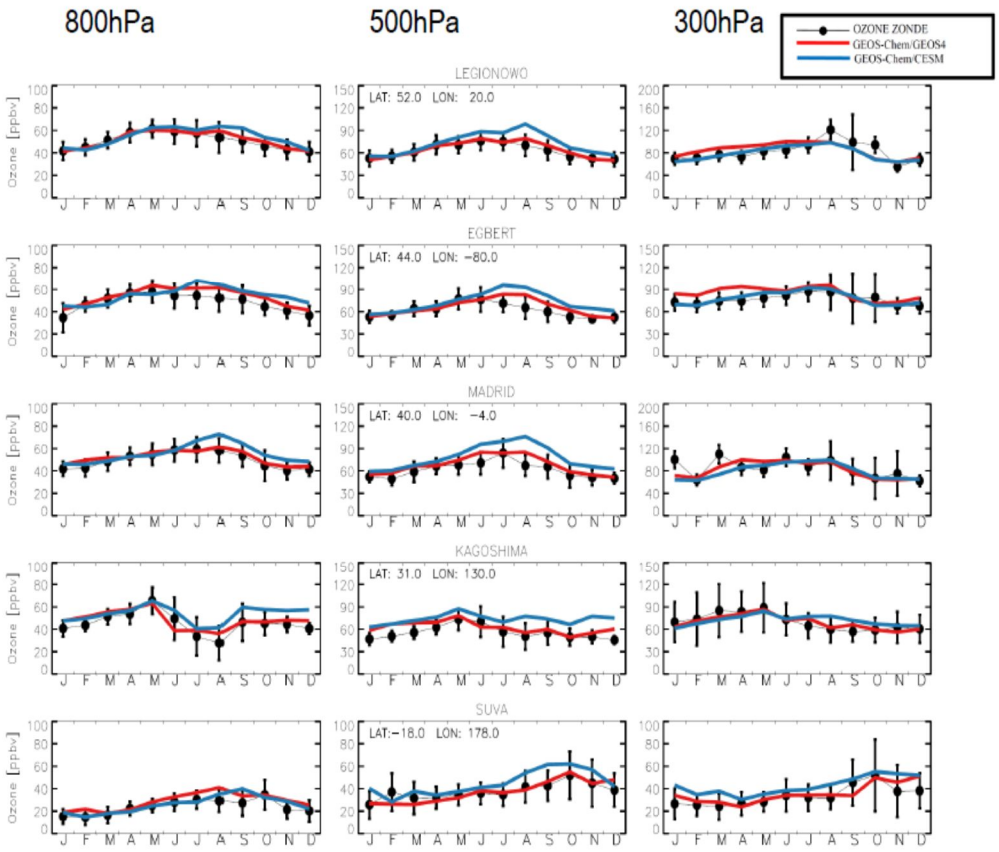

Fig. 3.2. Comparisons of the observed and simulated monthly mean concentrations of ozone at 800 hPa (left), 500 hPa (middle), and 300 hPa (right) at selected ozone sonde sites (Legionowo, Madrid, Egbert, Kagosima, and Suva). Black closed circles indicate WOUDC ozone sonde observations averaged for 1996–2005, and one standard deviation is denoted with the vertical bar. Blue and red solid lines are GEOS-Chem results driven by the CESM and GEOS-4 meteorology, respectively. Note the difference in scale among the panels.

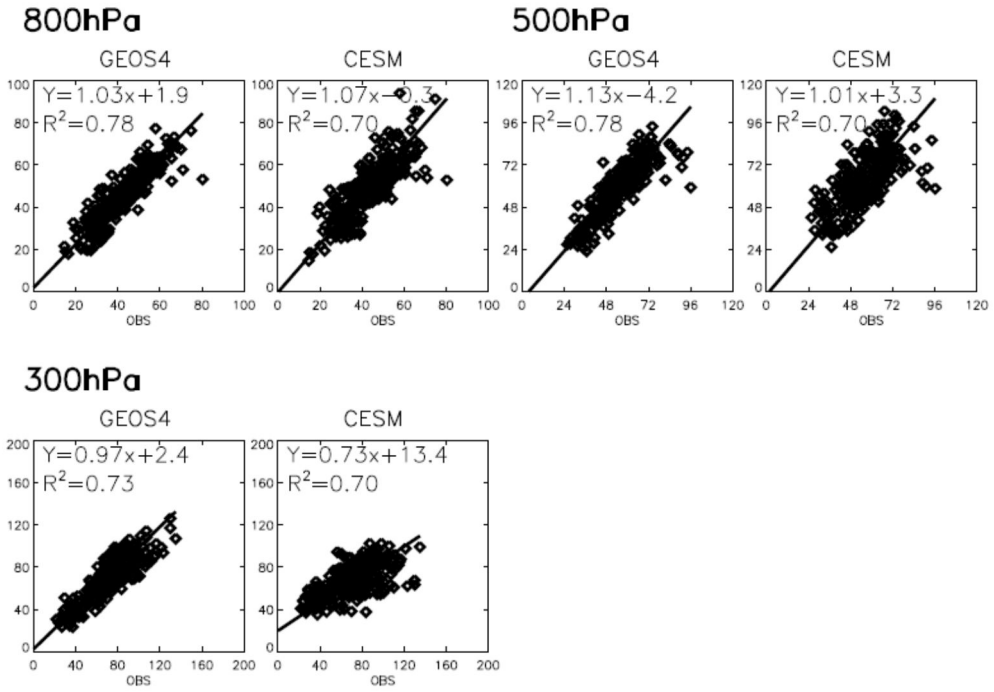

Fig. 3.3. Scatter plot comparisons of the observed versus simulated monthly mean concentrations of ozone at 800, 500, and 300 hPa at all WOUDC ozone sonde sites. The simulated results are from the GEOS-Chem simulations driven by the CESM and GEOS-4 meteorology.

Table 2.2. Distribution of the ozone burden throughout the troposphere in 2000. The unit is Tg and the parenthesis indicates the percentage of regional burden relative to the total tropospheric burden (321 Tg).

Tg	90°S-30°S	30°S-EQ	EQ-30°N	30°N-90°N
0-250 hPa		19.2 (6.0)	20.2 (6.3)	
250-500 hPa	32.1 (10.0)	23.1 (7.2)	23.4 (7.3)	45.9 (14.3)
500-700 hPa	14.4 (4.5)	16.4 (5.1)	19.2 (6.0)	26.7 (8.3)
700-1000 hPa	15.5 (4.8)	16.1 (5.0)	21.9 (6.8)	26.9 (8.4)

3.4 Future ozone under the RCP scenarios

This section presents my estimates of future ozone changes under the RCP scenarios. Figure 3.4 shows the 2000–2050 annual mean surface ozone changes for each RCP scenario. Values are negative indicating that the surface ozone in 2050 is lower than that of 2000 under the RCP2.6, RCP4.5, and RCP6.0 scenarios due to the reduction of anthropogenic emissions. The surface ozone concentration only increases under the RCP8.5 scenario mainly driven by the methane increase (from 1750 to 2800 ppbv). Previous multi model results also showed surface ozone enhancements under the RCP8.5 scenario due to the methane doubling (Young et al., 2013, IPCC, 2013). The 2000–2050 surface ozone changes averaged over the globe are 2.1, -3.3, -3.7, and -4.2 ppbv for RCP8.5, RCP6.0, RCP4.5, and RCP2.6, respectively. My estimates are consistent with those of previous studies (Szopa et al., 2013, Butler et al., 2012, Kawase et al., 2011). For example, Lamarque et al. (2011) showed that the reduction in NOx emissions in RCP2.6, RCP4.5 and RCP 6.0 resulted in decreases of surface ozone concentrations in 2100 relative to 2000. In contrast, the RCP8.5 projection caused a slight increase of ozone by ~5 ppbv. The ozone burden changes in this study are 22, -6, -9, and -29 Tg for RCP8.5, RCP6.0, RCP4.5, and RCP2.6, respectively, which are within the range of ACCMIP multi

modeling estimates of 20, -1, 7, and -18 Tg for 2030 and 57, -28, -25, and -61 Tg for 2100 (Young et al., 2013, IPCC, 2013, Lamarque et al., 2013b).

Ozone air quality is typically measured by the number of days exceeding the air quality standard (8-h maximum averaged ozone >60 ppbv). I estimate the probability of ozone air-quality exceedance for each RCP scenario over Europe, North America, and East Asia in Table 3.3. High ozone episodes decrease in the most scenarios in 2050 relative to 2000 except for the RCP8.5 scenario. The most significant reductions of 89% and 78%, reflecting large decreases in anthropogenic emissions in 2050, occur in Europe and North America. High-ozone episodes in East Asia also decrease by 43%, implying improved ozone air quality in the future but to a lesser degree relative to other regions. The frequencies of high ozone episodes in RCP8.5 are similar to the present level due to the compensation between the anthropogenic emission decrease and the methane increase. This result is consistent with the previous study by Gao et al. (2013) who showed 57-86% decreases of high ozone episodes over North America under the RCP4.5 scenario. However, the frequencies of high-ozone episodes are comparable to those of 2000 under the RCP8.5 scenario (-37-23% changes).

In order to find the relation between the ozone precursors and ozone concentration changes in 2050, I calculate correlation coefficients between the

2000–2050 change of each ozone precursor emission (NO_x and VOCs) and the 2000–2050 change of high ozone episode days using the results of all RCP scenarios. Regional mean values are first computed and then used to compute correlation coefficients for different regions: Europe (10°E–30°E, 35°N–55°N), North America (70°W–125°W, 30°N–50°N), and East Asia (100°E–130°E, 20°N–50°N). I generally find high correlation coefficients between NO_x emission and high ozone probability (R = 0.43, 0.93, and 0.99 in East Asia, North America, and Europe, respectively) but low or negative correlation coefficients between VOC emission and high ozone probability (R = 0.00, -0.65, and -0.07 in East Asia, North America, and Europe). In 2050, anthropogenic VOC emission decreases, but this decrease is compensated by BVOC emission increase owing to temperature increase, resulting in low or negative correlations with ozone change. The results indicate that NO_x rather than VOC emission change will likely regulate future ozone air quality.

The RCP scenarios explicitly consider varying levels of legislation, economic growth, and technological progress across regions, resulting in regionally different developments for emission intensities. Nevertheless, the emissions of greenhouse gases generally increase in the future and the pollutant emissions including NO_x and VOCs are significantly reduced due to legislation and technological shifts after 2030 (Riahi et al., 2011). This inconsistency

between future emissions of greenhouse gas increases and air pollutant decreases in the RCP scenarios has some limitations to predict future air quality (Yan et al., 2014).

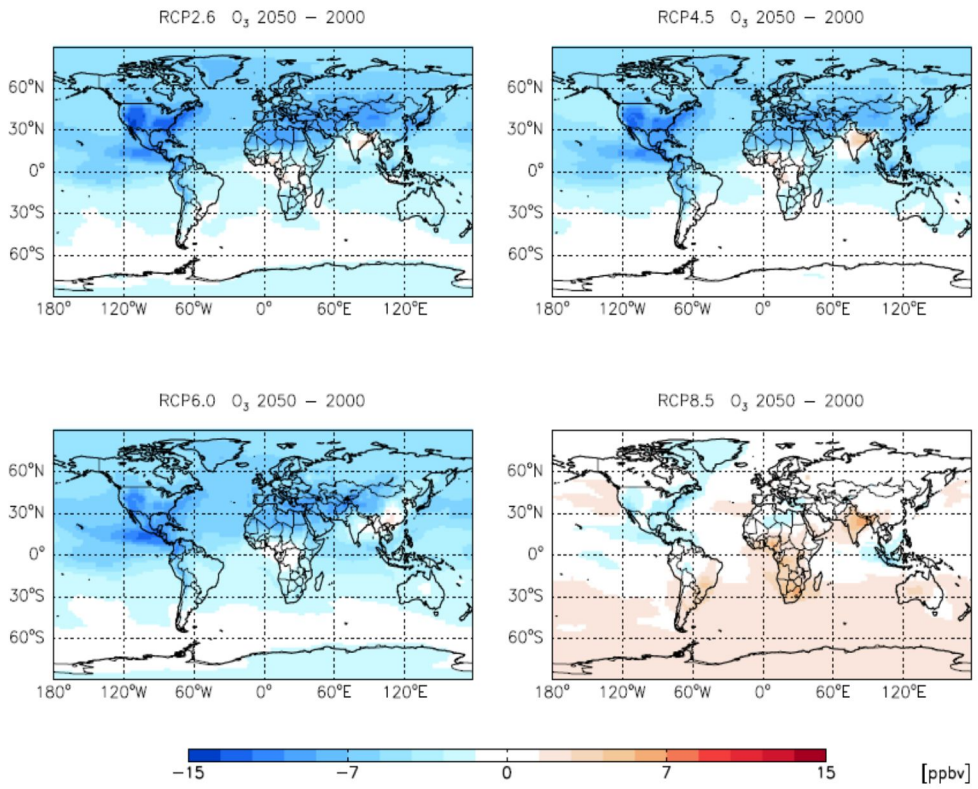

Fig. 3.4. Annual mean surface ozone changes for RCP 8.5, RCP 6.0, RCP 4.5, and RCP 2.6 scenarios between 2000s and 2050s. Simulated 2000–2050 changes in annual mean surface ozone changes for RCP2.6 (upper left), RCP4.5 (upper right), RCP6.0 (lower left), and RCP8.5 (lower right) scenarios.

Table 3.3. Simulated annual high ozone episode probabilities in Europe (10°E–30°E, 35°N–55°N), North America (70°W–125°W, 30°N–50°N), and East Asia (100°E–130°E, 20°N–50°N) under the 2000 and 2050 scenarios. Probabilities are defined as high ozone episodes days (8-h maximum averaged ozone is greater than 60 ppbv) divided by the total days. A high ozone probability is first computed for each grid using 10-yr simulation results for each scenario, and regional mean values are obtained by averaging grid-values for each region.

	Europe	North America	East Asia
2000	10.5	10.2	17.1
RCP2.6 2050	1.2	0.2	5.8
RCP4.5 2050	1.9	0.4	5.9
RCP6.0 2050	1.8	1.0	6.8
RCP8.5 2050	10.1	8.7	17.2

3.5 Attribution of ozone change to meteorological variables

This section investigates the effect of climate change on ozone air quality, particularly under the RCP8.5 scenario. For this purpose, I conduct a sensitivity simulation for 2049–2051 to examine the effect of climate changes alone on ozone air quality, assuming no changes in anthropogenic ozone precursor emissions from the present-day values in section 3.3. To isolate the effects of climate change, methane concentrations are also fixed at the 2000 level. Therefore, all the ozone changes here are solely due to future meteorology changes. Future climate is driven by the change in long-lived greenhouse gas emissions. I use the statistical method discussed in section 3.2 to analyze the results to quantify the effect of each meteorological variable on ozone concentrations in 2050.

I focus my analysis on seasonal mean ozone in summer, for which the 2000–2050 changes are shown in Fig. 3.5. Values increase in the polluted continents. The peak increase of 3.2 ppbv occurs in Europe, but North America and East Asia also experience ozone increases of 1.9 and 0.4 ppbv. In contrast, ozone over the ocean decreases, especially in the Northern Hemisphere.

The simulated ozone change can be explained by a change of meteorological condition that is a combination of multi-variable changes. In

order to find key meteorological variables for the ozone change, I use the correlation and partial-correlation analyses between ozone and meteorological variables (cloud fraction, PBL height, temperature, zonal wind, meridional wind, specific humidity, pressure, and convective mass flux) in surface air, as shown in Figure 3.6. This information is important for air quality prediction and the mitigation strategy development. Key meteorological variables for ozone could vary depending on different regions and climate conditions. In this study, however, I conduct this analysis over the globe simply for selecting variables applicable for the whole globe. Despite the global selection of variables, the application of my regression analysis below will be done based on the grid-mean values, which thus takes into account the grid-scale and further the large-scale change. A relationship change depending on regions and climate conditions would be a subject for a future study. Values in the figure are global mean correlation and partial correlation coefficients computed by taking the average of each grid value in surface air.

I find that ozone has the highest positive correlation with temperature (0.47), which is followed by the correlation with PBL height (0.44). On the other hand, the ozone change is anti-correlated with specific humidity and cloud fraction (R = -0.38 and -0.26). Wind, pressure, and convective mass flux show insignificant correlation (<0.1) with ozone. The partial correlation coefficients of

most variables are similar to the correlation coefficients, except for PBL height for which the value decreases to -0.04, indicating large dependency with other variables. Based on the analysis, I select 3 key variables: temperature, specific humidity, and cloud fraction. These variables are known to largely affect ozone air quality (Dentener et al., 2006, Meleux et al., 2007, Lin et al., 2008).

Using the selected variables as a predictor and the ozone change as the predictand, I construct multiple linear regression models (equation 3.4) for each grid after applying the Gram–Schmidt orthonormalization (equation 3.3) to the predictor variables. The linear regression model explains 63% of ozone variance globally. The rest of the variance indicates nonlinear effects and effects from other meteorological variables. Previous studies using a statistical model also showed that the linear regression model explained a similar magnitude (50–70%) of variance (Tai et al., 2010, Tai et al., 2012a, Abdul-Wahab et al., 2005).

Figure 3.7 shows the ozone change corresponding to each meteorological variable change. Temperature increase results in ozone increase over land. The positive correlation of ozone with temperature is due primarily to the increase in biogenic isoprene flux. The ozone increase is the highest in Europe (2.2 ppbv) and is high in North America (1.4 ppbv), but it is relatively small in East Asia (0.1 ppbv). The dissimilar regional ozone changes can be explained by the different increases in BVOC emissions in summer (12.1, 6.2,

and 3.5 TgC yr^{-1} for North America, Europe, and East Asia, respectively; shown in Fig. 3.8a), which are a function of temperature increases (3.8, 3.1, and 1.7^{o}C in North America, Europe, and East Asia, respectively). Europe and North America experience higher temperature increases than East Asia, which additionally contributes to the faster ozone production. Moreover, ozone in Europe appears to be more sensitive to BVOC emission change relative to the other regions. The simulated total VOC to NO_x ratio in summer is 2 in Europe (Fig. 3.8b), indicating that the severe VOC-limited regime in which BVOC emission increases because of the warmer temperature produces ozone more efficiently (Hedegaard et al., 2008, Meleux et al., 2007, Andersson and Engardt, 2010).

Ozone over the oceans in the Northern Hemisphere, however, is largely reduced with temperature increase, which is related with the effects of specific humidity shown in Fig 3.7b. Temperature increases enhance water evaporation from the oceans in the warming climate. The resulting increase in water vapor concentrations accelerates the destruction of ozone under the low-NO_x conditions of the oceans. The variances of temperature and specific humidity are positively correlated and affect ozone change together, and the effect of each variance is not clearly separable in my analysis. Instead, I estimate the covariance effect of the two variables as measured by the difference in the

explained variance of ozone between the regression models when alternating the order of the two predictor variables. Figure 3.7c shows the covariance effect of the two variables on ozone change, which is largely positive over land but negative over ocean.

Figures 3.7d and 3.7e show the effects of temperature and specific humidity on ozone change after removing the covariance effect. The temperature effect is largely an ozone increase everywhere, with a summertime mean increase of 0.51 ppbv, except for oceans downwind of continental outflows. This suppression of ozone might be due to accelerated thermal decomposition of PAN, which plays an important role in long-range transport of NO_x. My simulated surface PAN concentration is reduced by 15% over the Northern Hemisphere in 2050 relative to 2000. The effect of humidity on ozone is largely negative (Fig. 3.7b) and is concentrated mostly over the oceans where the summertime mean ozone decrease is 0.8 ppbv.

Doherty et al. (2013) examined the ozone responses to changes of climate conditions and suggested the enhanced peroxyacetyl nitrate (PAN) decomposition and isoprene emission over the land as major factors for ozone increase under the warming climate, while the increase of specific humidity had the opposite effect on ozone. My results are generally consistent with that of Doherty et al. (2013) that the ozone increase over the land can be explained by

the enhanced PAN decomposition and isoprene emission owing to the temperature increase (Fig. 3.7d). The ozone decrease over the ocean is due to the specific humidity increase (Fig. 3.7e).

Figure 3.7f indicates the effect of cloud change on ozone. The effect is not dominant globally, except in East Asia where ozone increases occur owing to cloud fraction decrease. However, I must acknowledge that the climate model prediction of cloud change is highly uncertain, despite its importance for future ozone change. In addition, the Asian summer monsoon and its change under future climate are a key factor determining ozone in East Asia, but this factor is also highly uncertain and needs to be investigated further (Gettelman et al., 2004, Park and Kim, 2014).

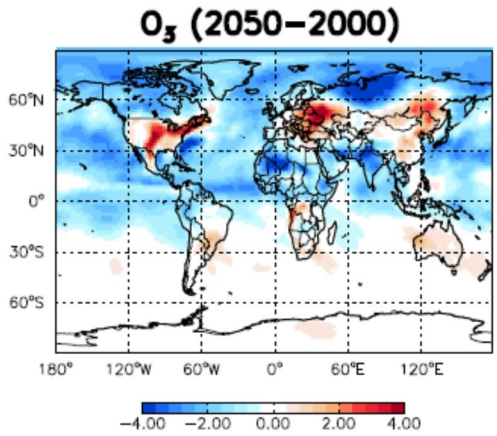

Fig. 3.5. Simulated 2000–2050 changes in summertime mean surface ozone for the RCP8.5 scenario assuming no changes in anthropogenic ozone precursor emissions and methane concentration from the present-day values.

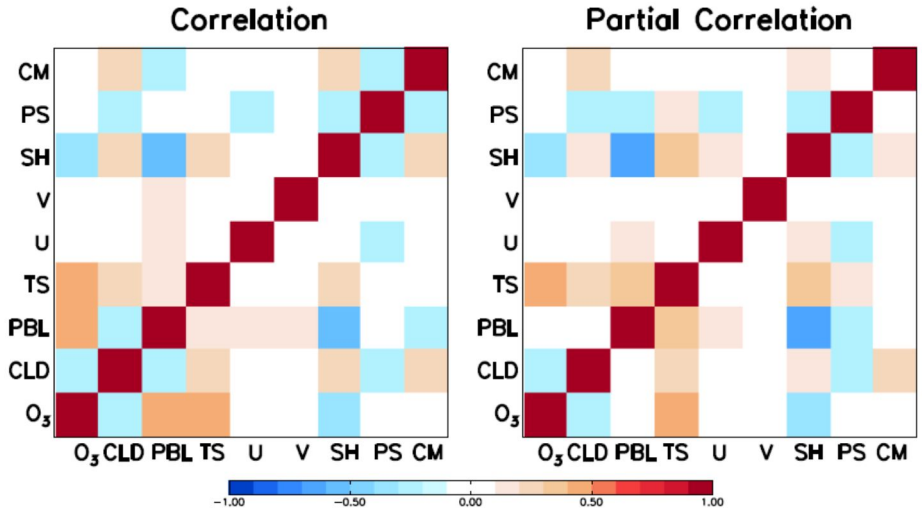

Fig. 3.6. Correlation and partial-correlation coefficients between ozone and individual meteorological variables: cloud fraction, PBL height, temperature, zonal wind, meridional wind, specific humidity, pressure, and convective mass flux in surface air. We use all values of model grid boxes at the surface for the statistical analysis.

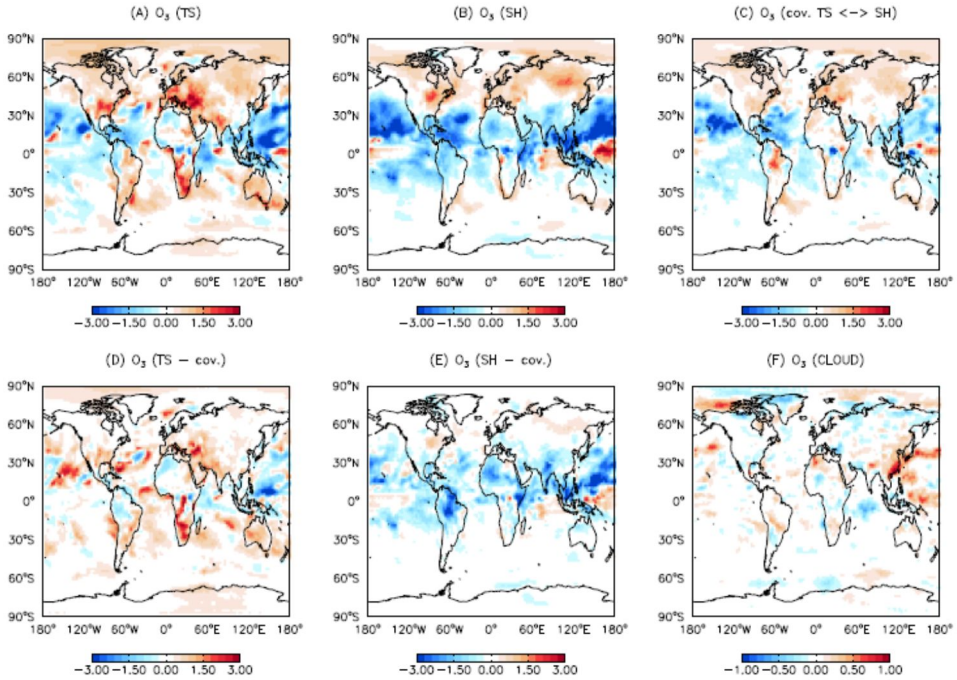

Fig. 3.7. 2000–2050 changes in summertime mean ozone concentration corresponding to each meteorological variable change. Each panel indicates the ozone change driven by changes of (a) temperature, (b) specific humidity, (c) covariance between temperature and specific humidity, (d) temperature alone, (e) humidity alone, and (f) cloud fraction. (d) and (e) show the ozone changes caused by temperature and specific humidity changes alone without the covariance effect between the two and are obtained by subtracting (c) from (a) and (b), respectively.

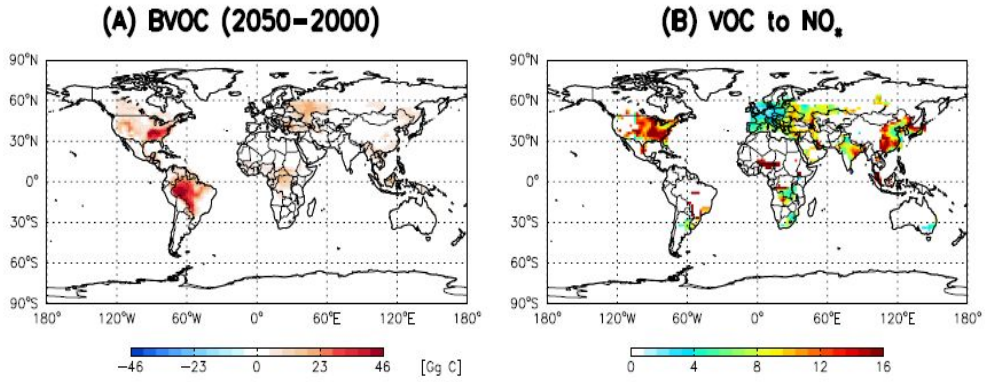

Fig 3.8. (a) Simulated 2000–2050 changes in summertime mean biogenic VOC emissions and (b) simulated summertime VOC to NOx ratio in 2000.

3.6 Effects of climate change on oxidants

3.6.1 OH change

Future climate change affects not only ozone concentrations but also the concentrations of other tropospheric oxidants. I now examine the effects of climate change on future OH concentrations. I use a sensitivity simulation result under the RCP8.5 scenario with methane doubling (2800 ppbv). I assume no changes in anthropogenic ozone precursor emissions from the present-day values in section 3.3. Figure 3.9a shows the 2000–2050 changes in annual mean OH

concentration in surface air without anthropogenic ozone precursor emission change except for methane, whose change follows RCP8.5. OH concentration generally decreases by 28% globally, reflecting a dominant loss of OH by the methane oxidation. This result is consistent with ACCMIP multi model results (Voulgarakis et al., 2013). Over the oceans, despite the increases of water vapor in RCP8.5, the dominant factor of driving OH changes is also the methane oxidation.

Voulgarakis et al. (2013) suggested that the stratospheric ozone recovery might decrease OH burden in the troposphere. However, they also concluded the surface OH decreases under RCP8.5 mostly due to methane increases. The effect of stratospheric ozone recovery on surface OH is low under RCP8.5.

$$\text{OPE} \equiv \frac{P_{O3}}{L_{O3}} = \frac{k_{HO2+NO}\,[HO_2][NO]}{k_{OH+NO2}\,[OH][NO_2]} \qquad \text{(R1)}$$

The change in OH also affects the Ozone Production Efficiency (OPE), defined by (R1). The OPE in 2050 is generally higher than that of the present, especially in the Southern Hemisphere where the value is increased by 32%. Despite the enhanced destruction of ozone by H_2O over the oceans in the future, the Southern Hemisphere shows ozone increase that is likely due to the OPE enhancement.

3.6.2 HNO_3 change

HNO_3 is a main sink of NO_x, and its deposition affects the ecosystem. I also examine the effects of climate change on future HNO_3 burden under the RCP 8.5. For this analysis, I also assume no changes in anthropogenic ozone precursor emissions from the present-day values except for methane (2800 ppbv). Figure 3.9c shows the change in the tropospheric HNO_3 burden between 2000 and 2050. I find that the HNO_3 burden increases by 8% in the future relative to the present. The peak increase of its concentration appears at mid- troposphere (500–600 hPa) in my model. Racherla and Adams (2008) previously showed that HNO_3 concentrations could increase in the future owing to the NO_2/NO_x ratio increase driven by increased ozone chemical production. I investigate this using my results and find that the NO_2/NO_x ratio increase can explain only a 1% global increase in HNO_3. Accelerated chemical reaction caused by the temperature increase contributes an additional 1.4% increase in the model. The increase by these two factors falls substantially short of the 8% increase in HNO_3 global burden.

I find that the HNO_3 burden enhancement is due primarily to natural NO_x emissions. Lightning and soil NO_x emissions are increased by 10% and 11%, respectively, in my simulations. Previous studies also showed similar future

increases in these natural NO_x emissions (Wu et al., 2008b, Kawase et al., 2011). When I conduct simulation without this natural-source change, the HNO_3 burden increase is only 3% and is largely due to NO_x partitioning and accelerated chemical reaction. The resulting HNO_3 deposition also increases from 88.4 Tg yr^{-1} to 92.2 Tg yr^{-1}, indicating that acid deposition might be exacerbated in future if the present level of ozone precursor emissions remains the same. However, nitrogen deposition will likely decrease because of the reduction of anthropogenic NO_x emissions, as projected by the RCP scenarios (Ellis et al., 2013, Lamarque et al., 2013a). However, my results indicate that increases in natural NO_x emissions might seriously offset future nitrogen deposition decreases from anthropogenic NO_x emission reduction.

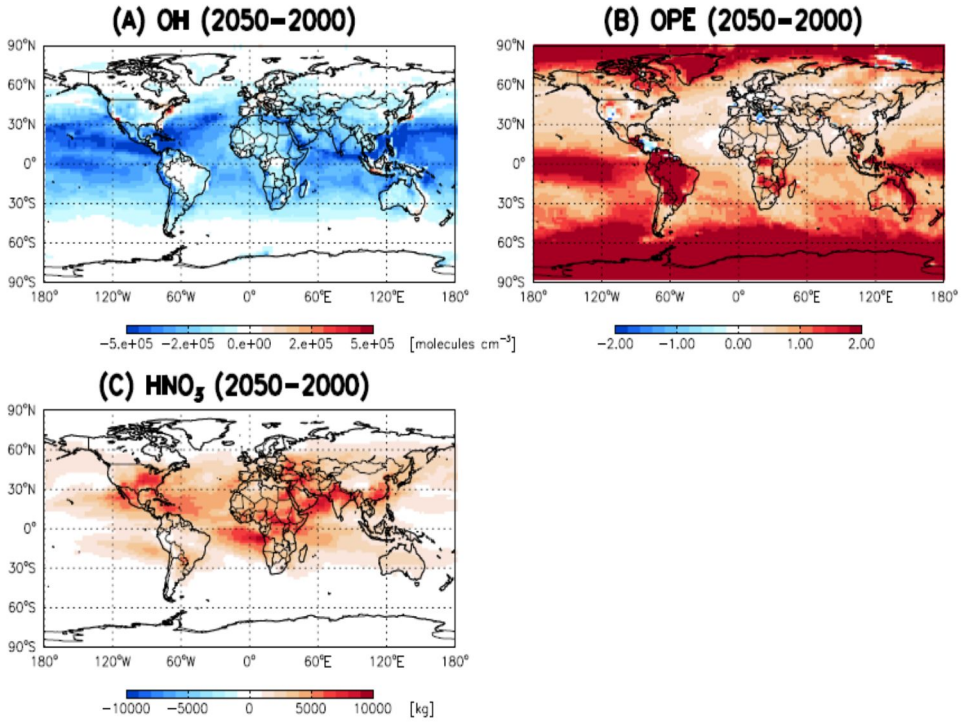

Fig. 2.9. Simulated 2000–2050 changes in annual mean (a) concentrations of OH in surface air, (b) ozone production efficiency in surface air, and (c) global HNO_3 burden.

3.7 Summary

I examined future air quality change focusing primarily on ozone concentrations in surface air. For this purpose, I updated GEOS-Chem to be driven by meteorological fields from the NCAR CESM. I first evaluated the model by focusing on observed climatological features of ozone concentration. The model well captured not only the spatial but also the temporal variation of the observed ozone concentrations.

I conducted model simulations using all the RCP scenarios to estimate future ozone changes. Global averages of 2000–2050 surface ozone change were 2.1, -3.3, -3.7, and -4.2 ppbv for RCP8.5, RCP6.0, RCP4.5, and RCP2.6, respectively, reflecting the large reduction of anthropogenic NO_x and VOCs emissions except for RCP8.5. Ozone increases under RCP8.5 are primarily due to the doubling of methane. High ozone episodes also decreased everywhere for most of scenarios in 2050 relative to the present. I found that the future ozone air quality would likely be regulated by NO_x rather than VOC emission changes.

I also investigated the effect of climate change on ozone air quality, particularly under the RCP8.5 scenario, by conducting sensitivity simulations with no changes in anthropogenic ozone precursor emissions and by applying statistical methods to the simulated results. My analysis revealed that the

temperature increase resulted in ozone increases over land of up to 2.2 ppbv in summer because of biogenic isoprene flux increase. Ozone over the oceans, however, was reduced with specific humidity increase mostly in the Northern Hemisphere, where the summertime mean ozone decrease is 0.8 ppbv. I also found that ozone concentrations were increased regionally by a cloud cover reduction in East Asia, where the summer monsoon plays an important role in determining ozone concentrations.

Future climate change affects not only ozone concentrations but also the concentrations of other tropospheric oxidants. I found that OH concentration generally decreases by 28% globally, reflecting a dominant loss of OH by the methane oxidation. The OPE in 2050 is 32% higher than that of 2000 in the Southern Hemisphere. Despite enhanced destruction of ozone by H_2O over the oceans in the future, the Southern Hemisphere shows an ozone increase that is likely due to the OPE enhancement. I also found that the HNO_3 burden is increased by 8% in the future relative to the present primarily because of an increase in natural NO_x emissions, which might seriously offset the future nitrogen deposition decrease caused by anthropogenic NO_x emission reductions.

CHAPTER Ⅳ

RELATIONSHIP CHANGES BETWEEN THE EAST ASIAN SUMMER MONSOON AND OZONE IN SURFACE AIR IN THE PRESENT AND FUTURE CLIMATE

4.1 Objective

The East Asian summer monsoon (EASM) has a significant impact on synoptic weather conditions in East Asia including winds, cloud covers, and precipitation (*Wang et al.,* 2004). Therefore, its relation with those weather variables has been under intense scrutiny over the past years to improve the predictability of weather and climate in East Asia (*Wang and Ding*, 2006).

Recent studies based on the observations and modeling have shown that the EASM has influences not only on synoptic weather but also on summer-time ozone air quality in East Asia (*He et al.*, 2008; *Yang et al.*, 2014; *Zhou et al.*,

2013). For example, the lowest summer surface ozone in East Asia typically occurred with the strong incursion of the EASM that transported clean oceanic air (*Pochanart et al.*, 2002; *Wang et al.*, 2006; *Yamaji et al.*, 2006; *Zbinden et al.*, 2006; *Zhou et al.*, 2013). The EASM not only affects the seasonal patterns of surface ozone over this region, but also results in the lowest summertime transport of pollutants during the year from the Asian continent to Japan and other regions because of the weak Asian outflow and northwestward penetration of the maritime air mass (*Yamaji et al.*, 2006; *Zbinden et al.*, 2006). Furthermore, *Tanimoto et al.* (2005) indicated that exchanges between continental and maritime air masses driven by the Asian monsoon play a central role in producing the latitudinal differences in ozone seasonality observed at Acid Deposition Monitoring Network in East Asia (EANET) sites.

Zhao et al. (2010) first introduced the impact of EASM on the ozone air quality over East Asia using the chemical transport model. They found that the monsoon system strongly modulates the pollution problem over a large portion of East China in the summer, depending on its strength and tempo-spatial extension. Their model results also suggested that transport from the stratosphere and long-range transport from East China and South/Central Asia all make significant contributions to ozone enhancements over West China. *Yang et al.* (2014) quantified the impacts of the East Asian summer monsoon on interannual

variations of June-July-August (JJA) surface-layer ozone concentrations using assimilated meteorological fields and GEOS-Chem chemical transport model. They showed that ozone concentration averaged over all of China is found to correlate positively with the EASM index by a large correlation coefficient of +0.75, indicating that summertime ozone concentrations are lower (or higher) in weaker (or stronger) EASM years.

On the other hand, global monsoon precipitation is expected to increase over the Northern Hemisphere (*IPCC*, 2013; *Lee and Wang*, 2014), and EASM is also expected to increase in the future (*IPCC*, 2013; *Seo et al.*, 2013). The future EASM system change can have a significant impact on future ozone air quality over East Asia. Previous modeling studies of future ozone air quality mostly focus on emission changes in the future (*Butler et al.*, 2012; *Cionni et al.*, 2011; *Fiore et al.*, 2012; *IPCC*, 2013; *Kawase et al.*, 2011; *Szopa et al.*, 2013; *Young et al.*, 2013). Monsoon system change in a warming climate greatly influences the future ozone air quality. The impact of the EASM change on future ozone should be investigated.

Here I investigate the effect of future monsoon change on ozone. For this purpose, I run the global 3-D chemical transport model (GEOS-Chem) (*Bey et al.*, 2001) to be driven by meteorological fields from the NCAR CESM. I first evaluate the performance of my modeling system by comparing simulated versus

observed past monsoon simulations. I estimate the effect of EASM on ozone using the statistical method in the present condition. I then conduct model simulations for 2050 using RCP8.5 scenario to estimate future monsoon and ozone air quality. Then, I estimate the effect of future monsoon change on ozone using statistical analysis.

4.2 Methodology

4.2.1 Model simulation

I use GEOS-Chem chemical transport model driven by meteorology from Community Earth System Model (CESM). Detailed model structure and evaluation results are described in *Kim et al.* (2015). I use GEOS-Chem version 8-01-03, which includes a fully coupled treatment of tropospheric O_3–NO_x–VOCs chemistry and aerosols (*Park et al.*, 2004). I also use CESM version 1.0.4. The model consists of Community Atmosphere Model 4 for the atmosphere and Community Land Model 4 with Carbon Nitrogen model for land. Parallel Ocean Program 3 and Community Ice Sheet Model 2 are used for ocean and sea ice calculation, respectively. The simulated output has a horizontal resolution of 2.0°

x 2.5° and 26 sigma levels. To account for interannual variability, the GEOS-Chem simulations are conducted for 10 years, 1996–2005 for the present-day climate (2000) under historical simulation and 2046–2055 for the future climate (2050) under RCP 8.5 scenario. I use the emissions compiled by *Choi et al.* (2014), who calculated 1995–2055 anthropogenic (including ship and aircraft) and biomass-burning emissions of ozone precursors based on the reference data of RCP emissions (RCP database online at http://tntcat.iiasa.ac.at:8787/RcpDb/dsd?Action= htmlpage&page=compare). Detailed simulation and emission information is also explained in *Kim et al.* (2015).

4.2.2 East Asia monsoon index

I use the reanalysis datasets and the model simulation to explore the effect of EASM on ozone air quality. The National Centers for Environmental Prediction (NCEP)/Department of Energy (DOE) reanalysis II (RA2) datasets (*Kanamitsu et al.*, 2002) are analyzed, and I also use the Global Precipitation Climatology Project (GPCP) monthly precipitation dataset version 2.2 for 1996-2005 (*Adler et al.*, 2003). Many of the EASM indices based on atmospheric thermodynamics and dynamics, such as pressure, ocean-land temperature contrast, wind field, and precipitation, have been widely used to quantify

monsoon extent and variability over monsoon regions (*Wang et al.*, 2009). In the present study, I use the definition of the EASM index of *Li and Zeng* (2002) using the NCEP DOE RA2 dataset, which is referred to as the observation. The EASM index is defined as follows:

$$\text{EASM index} = \frac{||\overline{\text{V}}_W - \text{V}_i||}{||\overline{\text{V}}||} - 2,$$

where $\overline{\text{V}}_W$ and V_i are the reference climatological winter wind vector and monthly wind vector at point i, respectively, and $\overline{\text{V}} = (\overline{\text{V}}_W + \overline{\text{V}}_S)/2$ is the climatological mean wind vector. In this study, $\overline{\text{V}}_S$ is the climatological summer wind (for the Northern Hemisphere, taking $\overline{\text{V}}_W = \overline{\text{V}}_{Jan}$ and $\overline{\text{V}}_S = \overline{\text{V}}_{Jul}$). The norm ||A|| is defined as follows:

$$||\text{A}|| = \left(\iint_S |A|^2 \, dS \right)^{1/2},$$

where S denotes the domain of integration. According to *Li and Zeng* [2002], the domain of the EASM index is defined as 10- 40°N and 110 – 140°E. This monsoon index has also been used in previous studies (*Li and Zeng*, 2003; *Nan and Li*, 2003; *Zhu et al.*, 2012) and by the NOAA Climate Prediction Center (http://www.cpc.ncep.noaa.gov/products/Global_Monsoons/Asian_Monsoons/monsoon_index.shtml). There is an apparent negative correlation between the

EASM index and rainfall variability in the middle and lower valley of the Yangtze River in China during the boreal summer (JJA), indicating that drought years over the valley are associated with a strong EASM and flood years with a weak EASM (*Nan and Li*, 2003).

4.3 Model evaluation

The ozone simulation of GEOS-Chem is massively evaluated in previous studies (*Alvarado et al.*, 2010; *Jeong and Park*, 2013; *Kim et al.*, 2013). The ozone simulation of GEOS-Chem driven by meteorological fields from the NCAR CESM is also evaluated in *Kim et al.* (2015). They evaluated the model by focusing on observed climatological features of ozone concentration. The model effectively captured not only the spatial but also the temporal variation of the observed ozone concentrations. I also use the identical model simulation result from *Kim et al.* [2015].

I compare the mean precipitation and low-level (850hPa) winds during JJA in the observations with those simulated in the CESM for 1996-2005 (Figs. 4.1 a, b) to examine the effect of summer monsoon on ozone. The GPCP precipitation is the highest around the Philippines and Northern Mariana Islands.

The second peak is located around southern China, Japan, and Korea, and is associated with the Baiu/Meiyu/Changma front (*Wang et al.*, 2004). On the other hand, the observed wind shows clear cyclonic circulation over southern Asia and southern China along with the southwesterlies from the ocean onto the land and anticyclonic circulation over the western North Pacific.

The CESM reasonably captures the overall pattern of mean precipitation and low-level winds during JJA compared to the observations. In particular, the precipitation band from southwestern China to the Korean peninsula is captured. However, some discrepancies exist in the detailed structures between the simulation and the observation. The overall amount of precipitation and the strength of circulation simulated in the model are smaller and weaker than those in the observations, respectively. The magnitude of the precipitation band from southwestern China to the Korea peninsula is smaller than that of observation, and its position is shifted to the north in the model. Such model biases are also found in most of the CMIP3 and CMIP5 model participants (*Sperber et al.*, 2013).

I analyze the regressed wind and precipitation fields against the EASM index (Fig. 4.1c) for the simulated values and observed values to evaluate the monsoon feature in CESM. The regressed precipitation shows the clear peak around the Philippines and Northern Mariana Islands in GPCP. The regressed

wind shows clear cyclonic circulation over southern China in NCEP DOE RA2. These features are general meteorological patterns over East Asia and also shown in JJA averaging fields, which reflects the dominance of EASM in summer.

Fig. 4.1d shows the regressed wind and precipitation fields against the EASM in CESM. The regressed wind and precipitation capture those from the observed. The regressed precipitation shows the clear peak around the Philippines and Northern Mariana Islands. However, the strength of peak is lower than that observed. Simulated precipitation also captured the cyclonic circulation over southern China. Despite this difference, the spatial pattern of the precipitation variability associated with the EASM index in the CESM is not influenced much by such discrepancies compared to the observation.

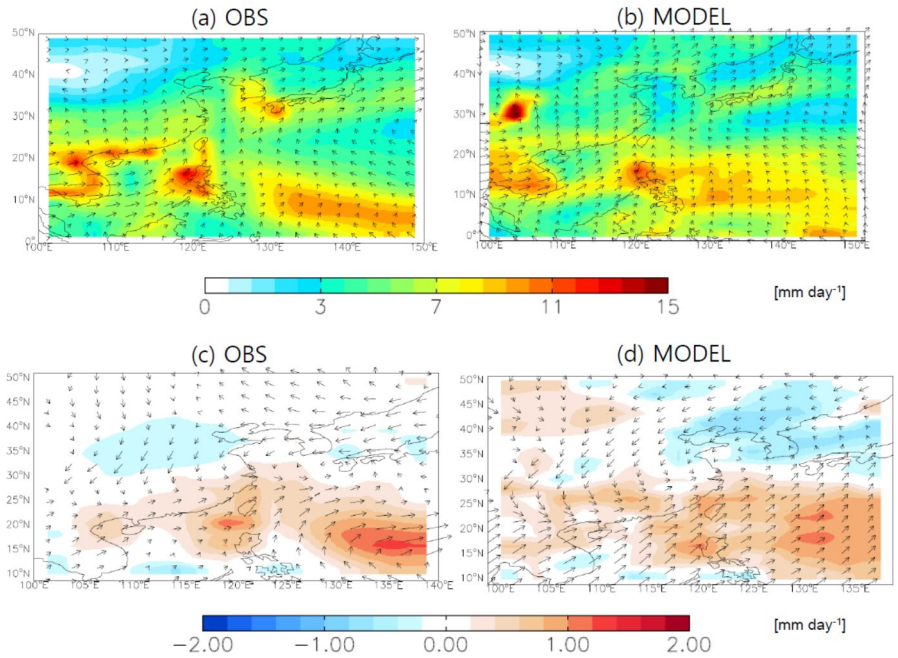

Fig. 4.1. (a) Boreal summer mean GPCP precipitation (shaded) and NCEP DOE RA2 wind fields at 850hPa (vector) for 1996-2005. (b) Same as (a) but for the CESM results. Unit is mm day^{-1}. (c) Regression of precipitation (shaded) and wind (vector) against the EASM index in the reanalysis data. (d) Same as (c) but for the CESM results. Unit is mm day^{-1}.

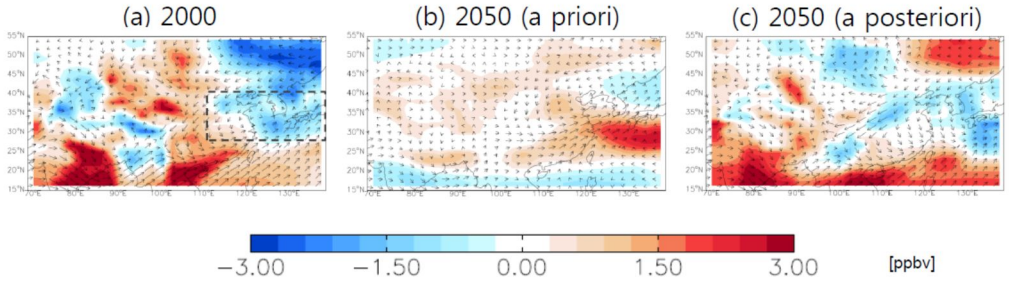

Fig. 4.2. (a) Regression of ozone (shaded) and wind (vector) against the EASM index from the model in 2000. (b) Same as (a) but for the 2050. (c) Same as (b) but for a posteriori result.

4.4 Effect of future monsoon change on ozone concentration

This section investigates the effect of future monsoon change on ozone air quality, particularly under the RCP8.5 scenario. I first estimate the effect of the monsoon on ozone air quality in the present. Fig. 4.2a shows the regressed ozone concentration against the EASM index in the model. The regressed ozone concentration is high in the China continent. The ozone is transported from Eastern China, which is a major source region that follows cyclonic monsoonal circulation. The regressed ozone concentration shows lower values over the Northern West Pacific and Japan affected by clean air from the Pacific. The ozone distribution patterns are the same as the previous study's results from *Yang et al.* (2014).

Then, I estimate the effect of the monsoon on ozone air quality in 2050 under the RCP8.5 scenario. Fig. 4.2b shows the regressed ozone concentration and wind field against the EASM index in 2050. For the wind, EASM circulation also shows the cyclonic circulation over Southern Asia and Southern China. However, the circulation center is shifted northward. This circulation shift makes the great change of regressed ozone concentration. The regressed ozone is high

at the downwind region including Southern Japan and the Northern Pacific in 2000 due to the outflow of Eastern China.

Fig. 4.3 a, b show time-series of EASM index and ozone concentration at Eastern China to Southern Japan (110–140°E, 30–40°N, dashed domain in Fig. 4.2a). There is a clear negative correlation in 2000, whereas there is a positive correlation in 2050 showing -0.60 and 0.23 respectively. These results indicate that the effect of the monsoon on ozone will be changed due to regional climate change. I find that the EASM index does not represent the EASM correctly in 2050. The regressed precipitation against the EASM index does not capture the precipitation peak over Philippines where the EASM precipitation is largest (Fig. 4.5a). Previous studies suggest that climate shift makes the change of EASM precipitation location and wind pattern (*Lee et al.*, 2010; *Zhisheng et al.*, 2015). Following the climate shift, the standard of EASM index should be changed. The EASM index from this study is calculated from wind difference between summer and winter at 850hPa. Fig. 4.4 shows the zonally averaged U wind difference between summer and winter over 110–140°E at 850hPa. I find that the location of maximum wind difference is shifted by 8° northward.

I newly define a domain of the EASM index considering wind shift as 10°N plus location change of maximum wind difference - 40°N plus location

change of maximum wind difference and 110–140°E. The domain of the EASM index in this case is defined as 18°N– 48°N and 110–140°E. The regressed precipitation effectively captures the high precipitation around the Philippines after changing the domain (Fig. 4.5b). The wind circulation center is shifted southward that has similar vortex center that of 2000. These results show that the new EASM index calculation effectively represents the EASM. These results also imply that calculation of the EASM index in the future calculation method should be changed due to climate change suggested by previous studies.

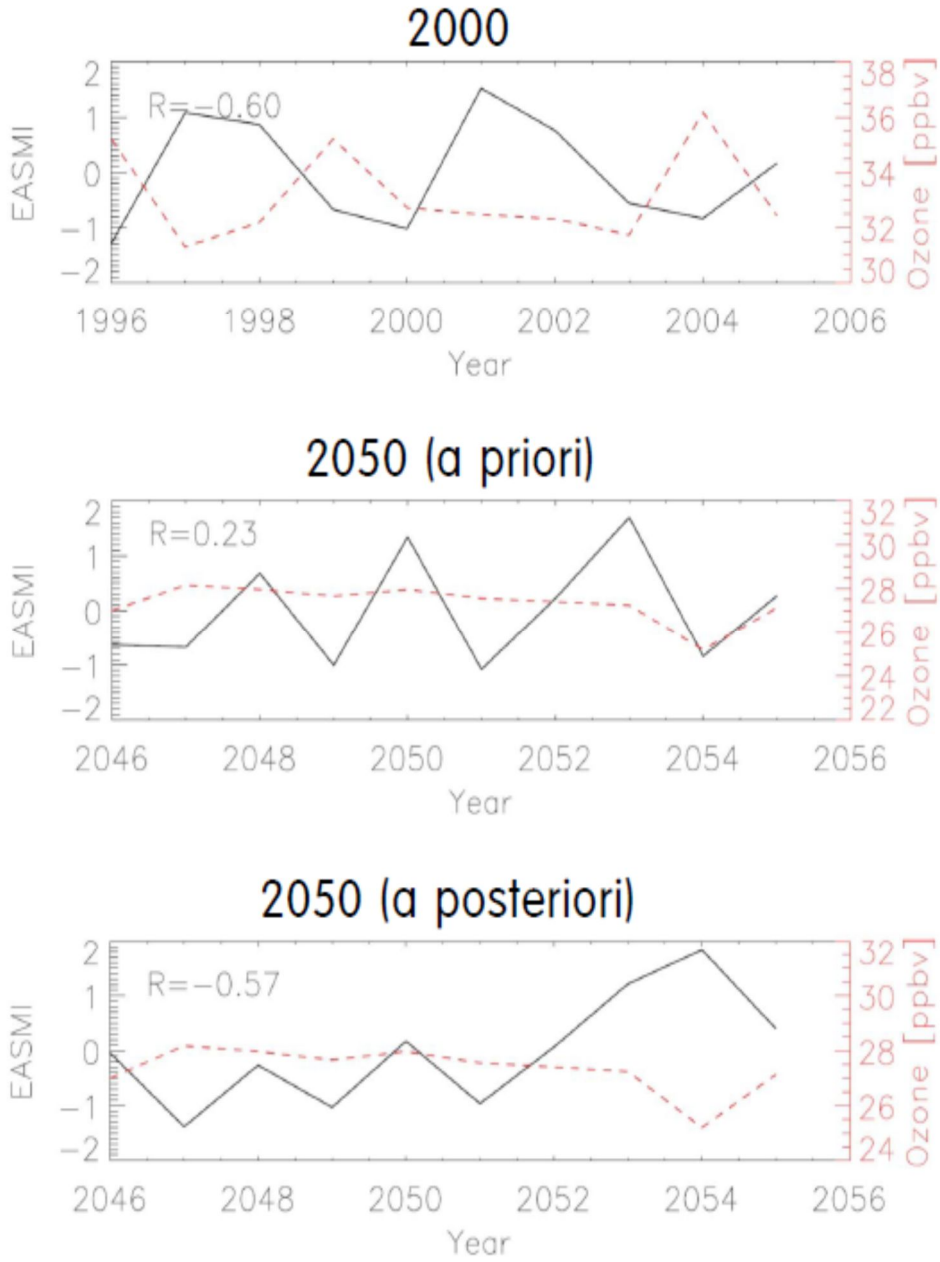

Fig. 4.3. Time-series of the EASM index (black) and ozone concentation over downwind region (110 – 140°E, 30 – 40°N) in 2000. (b) Same as (a) but for the 2050. (c) Same as (b) but for a posteriori result.

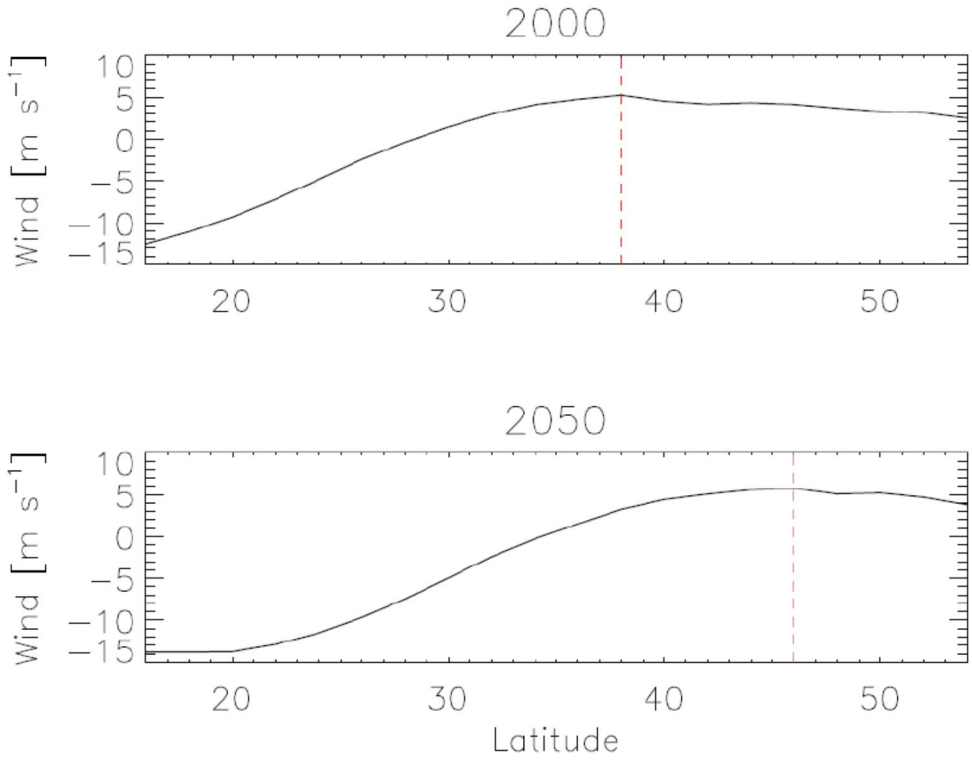

Fig. 4.4. (a) Zonally averaged U wind difference between JJA and January in 2000 at 850hPa over 100-140°E. (b) Same as (a) but for the 2050.

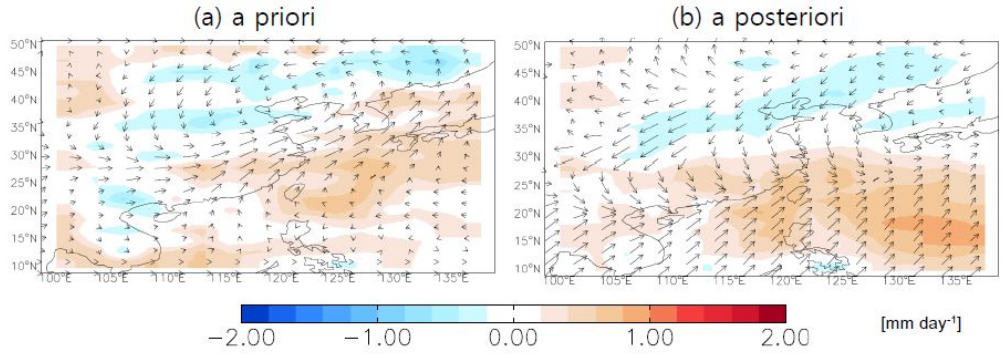

Fig. 4.5. (a) Regression of precipitation (shaded) and wind (vector) against the EASM index in 2050. (b) Same as (a) but for a posteriori result.

Fig. 4.2c shows the newly calculated regressed ozone concentration and wind field against EASM index. The regressed ozone field is low in the downwind region. The correlation between the EASM index and downwind ozone shows clear negative correlation showing -0.57 (Fig. 4.3c). This result indicates that different ozone patterns between 2000 and 2050 are mostly due to inappropriate domain selection for the EASM index. However, the magnitude of the ozone decrease in the downwind region is reduced. Time-series of the downwind ozone also shows small change. Nevertheless, the strength of monsoon varies largely from year to year.

The reduction of ozone change from EASM owes to weakening of monsoonal anticyclonic circulation over East Asia. Fig. 4.6 shows averaged vorticity over East Asia (110–140°E, 30–40°N). The vorticity has negative correlation against EASM index as follows by anticyclonic flow for both 2000 and 2050. The standard deviation of EASM indices are similar in 2000 and 2050 (0.97 and 0.93), however, the standard deviation of vorticity in 2050 is much lower than that of 2000 (0.77 and 0.40). The results indicate that the weak ozone transport from the Pacific Ocean creates the reduction of ozone change from EASM in 2050. The regressed easterly-westerly flux (EW-flux) of ozone against

EASM also shows consistent results (Fig. 4.7). The EW-fluxes of ozone are easterly flow over 35–40°N, and westerly over 20–25°N due to anticyclonic flow over East Asia. The patterns are consistent between 2000 and 2050; however, magnitude of EW-flux in 2050 is 40% lower than that of 2000. The results imply that ozone change over East Asia from EASM may decrease in 2050 owing to monsoonal circulation weakening over East Asia.

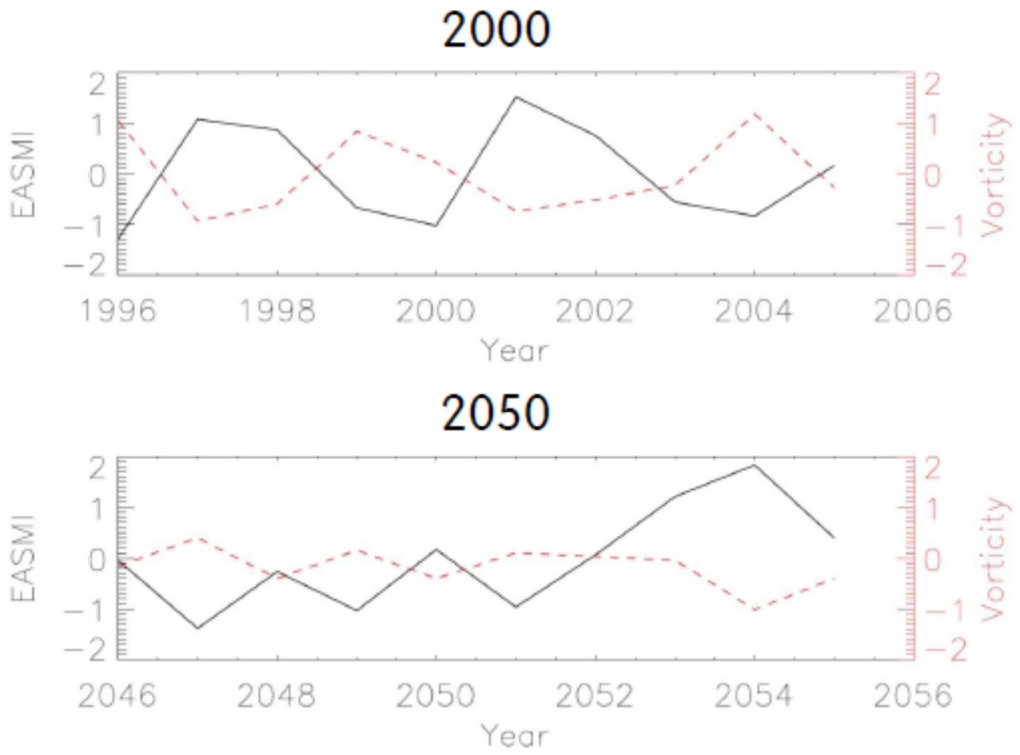

Fig. 4.6. Time-series of the EASM index (black) and vorticity over downwind region (110 – 140°E, 30 – 40°N) in 2000. (b) Same as (a) but for the 2050.

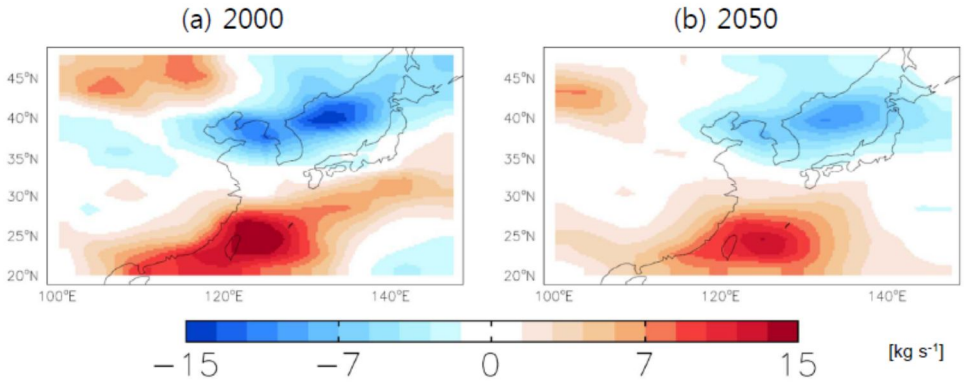

Fig. 4.7. (a) Regression of EW-flux against the EASM index from the model in 2000. (b) Same as (a) but for the 2050.

4.5 Summary

I examined effect of monsoon change on ozone focusing primarily over East Asia in surface air. For this purpose, I used GEOS-Chem to be driven by meteorological fields from the NCAR CESM. I first evaluated the model by focusing on observed climatological features of EASM. The model effectively captured spatial variation of observed precipitation and wind in the summertime. Then, I compare regressed wind and precipitation against EASM index. The model also captures the observed patterns.

I conducted model simulations using the RCP8.5 scenario to estimate effects of monsoon on ozone 2000 and 2050. I calculate the regressed ozone concentration against the EASM index to examine effects of monsoon on ozone. The regressed ozone concentration is high in China continents. The ozone is transported from Eastern China where the major source region follows cyclonic monsoon circulation. The regressed ozone concentration shows lower values over the Northern West Pacific and Japan affected by clean air from the Pacific. My results are comparable to the previous study's result from *Yang et al.* (2014).

Then I investigated the effect of monsoons on ozone air quality in 2050 under RCP8.5 scenario. The regressed ozone against EASM index in 2050 is totally different from that of 2000. I revealed that the difference of ozone response between 2000 and 2050 is due to EASM domain shift under the warming future climate. The difference of the ozone change between 2000 and 2050 is reduced when I correct the standard of EASM index. However, the ozone decrease in the downwind region is reduced in 2050. I found that the weak ozone response in 2050 is associated with a weakening of cyclonic circulation from EASM over East Asia in 2050. These results indicate that ozone response from the EASM forcing may change under the global warming climate.

CHAPTER Ⅴ

CONCLUSION

The changing climate and air quality are strongly connected to each other. Ozone and particle matters are strongly influenced by climate change. Air pollution can also impact the climate. However, understanding of interaction between climate change and air pollutants is still low. This dissertation is underway to address these uncertainties focusing on three objectives. (1) Future air quality under the RCP scenarios and attempt to reduce the associated uncertainty of future ozone projection. (2) The effect of aerosol on the East Asian summer monsoon using a long-term ensemble simulation. (3) The effect of the East Asian summer monsoon change on surface ozone concentration over East Asia under RCP8.5. In order to perform these studies, global 3-D chemical transport model and general circulation models were used to simulate air quality and climate conditions and to address uncertainties of understanding of interaction between climate change and air pollutants.

I examined future air quality change focusing primarily on ozone concentrations in surface air. For this purpose, I updated GEOS-Chem to be driven by meteorological fields from the NCAR CESM. I first evaluated the model by focusing on observed climatological features of ozone concentration.

The model well captured not only the spatial but also the temporal variation of the observed ozone concentrations. I conducted model simulations using all the RCP scenarios to estimate future ozone changes. Global averages of 2000–2050 surface ozone change were 2.1, -3.3, -3.7, and -4.2 ppbv for RCP8.5, RCP6.0, RCP4.5, and RCP2.6, respectively, reflecting the large reduction of anthropogenic NO_x and VOCs emissions except for RCP8.5. Ozone increases under RCP8.5 are primarily due to the doubling of methane. I also investigated the effect of climate change on ozone air quality, particularly under the RCP8.5 scenario, by conducting sensitivity simulations with no changes in anthropogenic ozone precursor emissions and by applying statistical methods to the simulated results. My analysis revealed that the temperature increase resulted in ozone increases over land of up to 2.2 ppbv in summer because of biogenic isoprene flux increase. Ozone over the oceans, however, was reduced with specific humidity increase mostly in the Northern Hemisphere, where the summertime mean ozone decrease is 0.8 ppbv. I also found that ozone concentrations were increased regionally by a cloud cover reduction in East Asia, where the summer monsoon plays an important role in determining ozone concentrations.

To examine the effects of sulfate aerosol forcing on the EASM, I conducted three sets of CAM5 model experiments including control run, SST-run, and SO_2-run. Each set of experiments was performed with four ensemble

members, the average of which was compared with the observations. The model reasonably captured the general patterns of precipitation and low-level winds over East Asia during JJA, although it failed to reproduce the detailed precipitation structures, reflecting the deficiency of the present global models. My analysis of the EASM index based on the observations showed that the intensity of the EASM has decreased over the past few decades. I found that both the control run and the SST-run reproduced such a weakening of the EASM. In contrast, the model with anthropogenic sulfate forcing showed a slight increasing trend of the EASM index, indicating that SST forcing has resulted in the weakening of the EASM, while the effect of regional sulfate aerosol forcing acts to strengthen the EASM for 1985-2010. The weakening of the EASM due to SST forcigns is mainly associated with the weakening of meridional temperature gradient for 2001-2010 along with the southward shift of the jet stream. This results in a downward motion at the right exit of the jet, causing a decrease in precipitation around 20ºN. On the other hand, the effect of sulfate aerosol forcing causes a cooling in southeastern China, which results in the weakening of the meridional temperature gradient in eastern China. As a result, the upper level jet stream decelerates at the jet exit region with the rising motion in southeastern. Consequently, an increase in precipitation around 18-23°N is induced by the effect of sulfate aerosol forcing over East Asia.

I examined effect of monsoon change on ozone focusing primarily over East Asia in surface air. For this purpose, I used GEOS-Chem to be driven by meteorological fields from the NCAR CESM. I first evaluated the model by focusing on observed climatological features of EASM. The model effectively captured spatial variation of observed precipitation and wind in the summertime. Then, I compare regressed wind and precipitation against EASM index. The model also captures the observed patterns. I conducted model simulations using the RCP8.5 scenario to estimate effects of monsoon on ozone 2000 and 2050. I calculate the regressed ozone concentration against the EASM index to examine effect of monsoon on ozone. The regressed ozone concentration is high in China continents. The ozone is transported from Eastern China where the major source region follows cyclonic monsoon circulation. The regressed ozone concentration shows lower values over the Northern West Pacific and Japan affected by clean air from Pacific. Then I investigated the effect of monsoon on ozone air quality in 2050 under RCP8.5 scenario. The regressed ozone against EASM index in 2050 is totally different with that of 2000. I revealed that the difference of ozone response between 2000 and 2050 is due to EASM domain shift under the warming future climate. The difference of the ozone change between 2000 and 2050 is reduced when I correct the standard of EASM index. However, the ozone decrease in the downwind region is reduced in 2050. I found that the weak ozone

response in 2050 is associated with a weakening of cyclonic circulation from EASM over East Asia in 2050.

REFERENCES

Abdul-Wahab, S.A., Bakheit, C.S., Al-Alawi, S.M., 2005. Principal component and multiple regression analysis in modelling of ground-level ozone and factors affecting its concentrations. Environmental Modelling & Software 20, 1263-1271.

Adler, R. F., et al. (2003), The Version-2 Global Precipitation Climatology Project (GPCP) Monthly Precipitation Analysis (1979–Present), Journal of Hydrometeorology, 4(6), 1147-1167, doi:10.1175/1525-7541.

Albrecht, B. A. (1989), Aerosols, Cloud Microphysics, and Fractional Cloudiness, Science, 245(4923), 1227-1230, doi:10.1126/science.245.4923.1227.

Alvarado, M.J., Logan, J.A., Mao, J., Apel, E., Riemer, D., Blake, D., Cohen, R.C., Min, K.E., Perring, A.E., Browne, E.C., Wooldridge, P.J., Diskin, G.S., Sachse, G.W., Fuelberg, H., Sessions, W.R., Harrigan, D.L., Huey, G., Liao, J., Case-Hanks, A., Jimenez, J.L., Cubison, M.J., Vay, S.A., Weinheimer, A.J., Knapp, D.J., Montzka, D.D., Flocke, F.M., Pollack, I.B., Wennberg, P.O., Kurten, A., Crounse, J., Clair, J.M.S., Wisthaler, A., Mikoviny, T.,

Yantosca, R.M., Carouge, C.C., Le Sager, P., 2010. Nitrogen oxides and PAN in plumes from boreal fires during ARCTAS-B and their impact on ozone: an integrated analysis of aircraft and satellite observations. Atmos. Chem. Phys. 10, 9739-9760.

Andersson, C., Engardt, M., 2010. European ozone in a future climate: Importance of changes in dry deposition and isoprene emissions. Journal of Geophysical Research: Atmospheres 115, D02303.

Banerjee, A., Archibald, A.T., Maycock, A., Telford, P., Abraham, N.L., Yang, X., Braesicke, P., Pyle, J., 2014. Lightning NOx, a key chemistry–climate interaction: impacts of future climate change and consequences for tropospheric oxidising capacity. Atmos. Chem. Phys. Discuss. 14, 8753-8778.

Bernard, S.M., Samet, J.M., Grambsch, A., Ebi, K.L., Romieu, I., 2001. The potential impacts of climate variability and change on air pollution-related health effects in the United States. Environmental Health Perspectives 109, 199-209.

Bey, I., Jacob, D.J., Yantosca, R.M., Logan, J.A., Field, B.D., Fiore, A.M., Li, Q., Liu, H.Y., Mickley, L.J., Schultz, M.G., 2001. Global modeling of

tropospheric chemistry with assimilated meteorology: Model description and evaluation. Journal of Geophysical Research D: Atmospheres 106, 23073-23095.

Brasseur, G.P., Schultz, M., Granier, C., Saunois, M., Diehl, T., Botzet, M., Roeckner, E., Walters, S., 2006. Impact of Climate Change on the Future Chemical Composition of the Global Troposphere. Journal of Climate 19, 3932-3951.

Butler, T.M., Stock, Z.S., Russo, M.R., Denier van der Gon, H.A.C., Lawrence, M.G., 2012. Megacity ozone air quality under four alternative future scenarios. Atmos. Chem. Phys. 12, 4413-4428.

Cionni, I., Eyring, V., Lamarque, J.F., Randel, W.J., Stevenson, D.S., Wu, F., Bodeker, G.E., Shepherd, T.G., Shindell, D.T., Waugh, D.W., 2011. Ozone database in support of CMIP5 simulations: results and corresponding radiative forcing. Atmos. Chem. Phys. 11, 11267-11292.

de Szoeke, S.P., Wang, Y., Xie, S.-P., Miyama, T., 2006. Effect of shallow cumulus convection on the eastern Pacific climate in a coupled model. Geophysical Research Letters 33, L17713.

Dentener, F., Stevenson, D., Ellingsen, K., van Noije, T., Schultz, M., Amann, M., Atherton, C., Bell, N., Bergmann, D., Bey, I., Bouwman, L., Butler, T., Cofala, J., Collins, B., Drevet, J., Doherty, R., Eickhout, B., Eskes, H., Fiore, A., Gauss, M., Hauglustaine, D., Horowitz, L., Isaksen, I.S.A., Josse, B., Lawrence, M., Krol, M., Lamarque, J.F., Montanaro, V., Muller, J.F., Peuch, V.H., Pitari, G., Pyle, J., Rast, S., Rodriguez, J., Sanderson, M., Savage, N.H., Shindell, D., Strahan, S., Szopa, S., Sudo, K., Van Dingenen, R., Wild, O., Zeng, G., 2006. The global atmospheric environment for the next generation. Environmental Science & Technology 40, 3586-3594.

Doherty, R.M., Wild, O., Shindell, D.T., Zeng, G., MacKenzie, I.A., Collins, W.J., Fiore, A.M., Stevenson, D.S., Dentener, F.J., Schultz, M.G., Hess, P., Derwent, R.G., Keating, T.J., 2013. Impacts of climate change on surface ozone and intercontinental ozone pollution: A multi-model study. Journal of Geophysical Research: Atmospheres 118, 3744-3763.

Ellis, R.A., Jacob, D.J., Sulprizio, M.P., Zhang, L., Holmes, C.D., Schichtel, B.A., Blett, T., Porter, E., Pardo, L.H., Lynch, J.A., 2013. Present and future nitrogen deposition to national parks in the United States: critical load exceedances. Atmos. Chem. Phys. 13, 9083-9095.

Eyring, V., Arblaster, J.M., Cionni, I., Sedláček, J., Perlwitz, J., Young, P.J., Bekki, S., Bergmann, D., Cameron-Smith, P., Collins, W.J., Faluvegi, G., Gottschaldt, K.D., Horowitz, L.W., Kinnison, D.E., Lamarque, J.F., Marsh, D.R., Saint-Martin, D., Shindell, D.T., Sudo, K., Szopa, S., Watanabe, S., 2013. Long-term ozone changes and associated climate impacts in CMIP5 simulations. Journal of Geophysical Research D: Atmospheres 118, 5029-5060.

Fiore, A.M., Naik, V., Spracklen, D.V., Steiner, A., Unger, N., Prather, M., Bergmann, D., Cameron-Smith, P.J., Cionni, I., Collins, W.J., Dalsoren, S., Eyring, V., Folberth, G.A., Ginoux, P., Horowitz, L.W., Josse, B., Lamarque, J.F., MacKenzie, I.A., Nagashima, T., O'Connor, F.M., Righi, M., Rumbold, S.T., Shindell, D.T., Skeie, R.B., Sudo, K., Szopa, S., Takemura, T., Zeng, G., 2012. Global air quality and climate. Chemical Society Reviews 41, 6663-6683.

Fujino, J., Nair, R., Kainuma, M., Masui, T., Matsuoka, Y., 2006. Multi-gas mitigation analysis on stabilization scenarios using aim global model. Energy Journal 27, 343-353.

Gao, Y., Fu, J.S., Drake, J.B., Lamarque, J.F., Liu, Y., 2013. The impact of

emission and climate change on ozone in the United States under representative concentration pathways (RCPs). Atmospheric Chemistry and Physics 13, 9607-9621.

Gent, P.R., Danabasoglu, G., Donner, L.J., Holland, M.M., Hunke, E.C., Jayne, S.R., Lawrence, D.M., Neale, R.B., Rasch, P.J., Vertenstein, M., Worley, P.H., Yang, Z.-L., Zhang, M., 2011. The Community Climate System Model Version 4. Journal of Climate 24, 4973-4991.

Gettelman, A., Kinnison, D.E., Dunkerton, T.J., Brasseur, G.P., 2004. Impact of monsoon circulations on the upper troposphere and lower stratosphere. Journal of Geophysical Research D: Atmospheres 109, 1-14.

Guenther, A., Karl, T., Harley, P., Wiedinmyer, C., Palmer, P., Geron, C., 2006. Estimates of global terrestrial isoprene emissions using MEGAN (Model of Emissions of Gases and Aerosols from Nature). Atmospheric Chemistry and Physics 6, 3181-3210.

Guo, L., E. J. Highwood, L. C. Shaffrey, and A. G. Turner (2013), The effect of regional changes in anthropogenic aerosols on rainfall of the East Asian Summer Monsoon, Atmos pheric Chemistry and Physics, 13(3), 1521-1534, doi:10.5194/acp-13-1521-2013.

Hack, J.J., 1994. Parameterization of moist convection in the National Center for Atmospheric Research community climate model (CCM2). Journal of Geophysical Research: Atmospheres 99, 5551-5568.

Haywood, J., and O. Boucher (2000), Estimates of the direct and indirect radiative forcing due to tropospheric aerosols: A review, Reviews of Geophysics, 38(4), 513-543, doi:10.1029/1999RG000078.

Hedegaard, G., Brandt, J., Christensen, J., Frohn, L., Geels, C., Hansen, K., Stendel, M., 2008. Impacts of Climate Change on Air Pollution Levels in the Northern Hemisphere with Special Focus on Europe and the Arctic, in: Borrego, C., Miranda, A. (Eds.), Air Pollution Modeling and Its Application XIX. Springer Netherlands, pp. 568-576.

Holtslag, A.A.M., Boville, B.A., 1993. Local Versus Nonlocal Boundary-Layer Diffusion in a Global Climate Model. Journal of Climate 6, 1825-1842.

Huang, Y., W. L. Chameides, and R. E. Dickinson (2007), Direct and indirect effects of anthropogenic aerosols on regional precipitation over east Asia, Journal of Geophysical Research: Atmospheres, 112(D3), D03212, doi:10.1029/2006JD007114.

IPCC, 2007. IPCC in Climate Change 2007: Impacts, Adaptations and Vulnerability.

IPCC, 2013. IPCC in Climate Change 2013: The Physical Science Basis.

Iwasaki, T., Kitagawa, and H. (1998), A possible link of aerosol and cloud radiations to Asian summer monsoon and its implication in long-range numerical weather prediction, Meteorological Society of Japan, Tokyo, JAPON.

Jacob, D.J., Winner, D.A., 2009. Effect of climate change on air quality. Atmospheric Environment 43, 51-63.

Jeong, J.I., Park, R.J., 2013. Effects of the meteorological variability on regional air quality in East Asia. Atmospheric Environment 69, 46-55.

Jiang, Y., X. Liu, X.-Q. Yang, and M. Wang (2013), A numerical study of the effect of different aerosol types on East Asian summer clouds and precipitation, Atmospheric Environment, 70(0), 51-63, doi:http://dx.doi.org/10.1016/j.atmosenv.2012.12.039.

Kanamitsu, M., W. Ebisuzaki, J. Woollen, S.-K. Yang, J. J. Hnilo, M. Fiorino,

and G. L. Potter (2002), NCEP–DOE AMIP-II Reanalysis (R-2), Bulletin of the American Meteorological Society, 83(11), 1631-1643, doi:10.1175/BAMS-83-11-1631.

Katragkou, E., Zanis, P., Kioutsioukis, I., Tegoulias, I., Melas, D., Krüger, B.C., Coppola, E., 2011. Future climate change impacts on summer surface ozone from regional climate-air quality simulations over Europe. Journal of Geophysical Research: Atmospheres 116, D22307.

Kawase, H., Nagashima, T., Sudo, K., Nozawa, T., 2011. Future changes in tropospheric ozone under Representative Concentration Pathways (RCPs). Geophysical Research Letters 38, L05801.

Kazimirovsky, E.S., Matafonov, G.K., 1998. Continental scale and orographic 'structures' in the global distribution of the total ozone content. Journal of Atmospheric and Solar-Terrestrial Physics 60, 993-995.

Kim, P.S., Jacob, D.J., Liu, X., Warner, J.X., Yang, K., Chance, K., Thouret, V., Nedelec, P., 2013. Global ozone–CO correlations from OMI and AIRS: constraints on tropospheric ozone sources. Atmos. Chem. Phys. 13, 9321-9335.

Komhyr, 1969. Electrochemical concentration cells for gas analysis. Annals of Geophysics 25, 203-210.

Kuhlmann, J., and J. Quaas (2010), How can aerosols affect the Asian summer monsoon? Assessment during three consecutive pre-monsoon seasons from CALIPSO satellite data, Atmos. Chem. Phys., 10(10), 4673-4688, doi:10.5194/acp-10-4673-2010.

Lamarque, J.-F., Kyle, G.P., Meinshausen, M., Riahi, K., Smith, S., van Vuuren, D., Conley, A., Vitt, F., 2011. Global and regional evolution of short-lived radiatively-active gases and aerosols in the Representative Concentration Pathways. Climatic Change 109, 191-212.

Lamarque, J.F., Dentener, F., McConnell, J., Ro, C.U., Shaw, M., Vet, R., Bergmann, D., Cameron-Smith, P., Dalsoren, S., Doherty, R., Faluvegi, G., Ghan, S.J., Josse, B., Lee, Y.H., MacKenzie, I.A., Plummer, D., Shindell, D.T., Skeie, R.B., Stevenson, D.S., Strode, S., Zeng, G., Curran, M., Dahl-Jensen, D., Das, S., Fritzsche, D., Nolan, M., 2013a. Multi-model mean nitrogen and sulfur deposition from the Atmospheric Chemistry and Climate Model Intercomparison Project (ACCMIP): evaluation of historical and projected future changes. Atmos. Chem. Phys. 13, 7997-8018.

Lamarque, J.F., Shindell, D.T., Josse, B., Young, P.J., Cionni, I., Eyring, V., Bergmann, D., Cameron-Smith, P., Collins, W.J., Doherty, R., Dalsoren, S., Faluvegi, G., Folberth, G., Ghan, S.J., Horowitz, L.W., Lee, Y.H., MacKenzie, I.A., Nagashima, T., Naik, V., Plummer, D., Righi, M., Rumbold, S.T., Schulz, M., Skeie, R.B., Stevenson, D.S., Strode, S., Sudo, K., Szopa, S., Voulgarakis, A., Zeng, G., 2013b. The Atmospheric Chemistry and Climate Model Intercomparison Project (ACCMIP): overview and description of models, simulations and climate diagnostics. Geosci. Model Dev. 6, 179-206.

Leibensperger, E.M., Mickley, L.J., Jacob, D.J., Chen, W.T., Seinfeld, J.H., Nenes, A., Adams, P.J., Streets, D.G., Kumar, N., Rind, D., 2012. Climatic effects of 1950–2050 changes in US anthropogenic aerosols – Part 1: Aerosol trends and radiative forcing. Atmos. Chem. Phys. 12, 3333-3348.

Li, J., and Q. Zeng (2002), A unified monsoon index, Geophysical Research Letters, 29(8), 115-111-115-114, doi:10.1029/2001GL013874.

Li, Q., Jacob, D.J., Park, R.J., Wang, Y., Heald, C.L., Hudman, R.C., Yantosca, R.M., Martin, R.V., Evans, M., 2005. North American pollution outflow and

the trapping of convectively lifted pollution by upper-level anticyclone. J. Geophys. Res. 110.

Li, J., and Q. Zeng (2003), A new monsoon index and the geographical distribution of the global monsoons, Advances in Atmospheric Sciences, 20(2), 299-302.

Lin, J.-T., Patten, K.O., Hayhoe, K., Liang, X.-Z., Wuebbles, D.J., 2008. Effects of Future Climate and Biogenic Emissions Changes on Surface Ozone over the United States and China. Journal of Applied Meteorology and Climatology 47, 1888-1909.

Lin, S.-J., Rood, R.B., 1996. Multidimensional Flux-Form Semi-Lagrangian Transport Schemes. Monthly Weather Review 124, 2046-2070.

Liu, Q., Lam, K.S., Jiang, F., Wang, T.J., Xie, M., Zhuang, B.L., Jiang, X.Y., 2013. A numerical study of the impact of climate and emission changes on surface ozone over South China in autumn time in 2000–2050. Atmospheric Environment.

Liu, X., et al. (2012), Toward a minimal representation of aerosols in climate models: description and evaluation in the Community Atmosphere Model

CAM5, Geoscientific Model Development, 5(3), 709-739, doi:10.5194/gmd-5-709-2012.

Liu, Y. U., J. Sun, and B. A. I. Yang (2009), The effects of black carbon and sulphate aerosols in China regions on East Asia monsoons, Tellus B, 61(4), 642-656, doi:10.1111/j.1600-0889.2009.00427.x.

Logan, J.A., 1999. An analysis of ozonesonde data for the lower stratosphere: Recommendations for testing models. Journal of Geophysical Research: Atmospheres (1984–2012) 104, 16151-16170.

Mao, J., Paulot, F., Jacob, D.J., Cohen, R.C., Crounse, J.D., Wennberg, P.O., Keller, C.A., Hudman, R.C., Barkley, M.P., Horowitz, L.W., 2013. Ozone and organic nitrates over the eastern United States: Sensitivity to isoprene chemistry. Journal of Geophysical Research: Atmospheres 118, 2013JD020231.

McLinden, C.A., Olsen, S.C., Hannegan, B., Wild, O., Prather, M.J., Sundet, J., 2000. Stratospheric ozone in 3-D models: A simple chemistry and the cross-tropopause flux. Journal of Geophysical Research: Atmospheres 105, 14653-14665.

Meehl, G.A., Washington, W.M., Arblaster, J.M., Hu, A., Teng, H., Tebaldi, C., Sanderson, B.N., Lamarque, J.-F., Conley, A., Strand, W.G., White, J.B., 2012. Climate System Response to External Forcings and Climate Change Projections in CCSM4. Journal of Climate 25, 3661-3683.

Meleux, F., Solmon, F., Giorgi, F., 2007. Increase in summer European ozone amounts due to climate change. Atmospheric Environment 41, 7577-7587.

Moon, N.K., Byun, D.W., Song, C.K., Park, R.J., 2004. A simple User's Guide for "geos2cmaq" code: Linking CMAQ with GEOS-CHEM, Version

1.0,"Interim report from Institute for Multidimensional Air Quality studies (IMAQS) University of Houston, TX.

[Available online at http://www.math.unh.edu/~dwbyun/Meetings/icap/].

Moorthi, S., Suarez, M.J., 1992. Relaxed Arakawa-Schubert. A Parameterization of Moist Convection for General Circulation Models. Monthly Weather Review 120, 978-1002.

Nan, S., and J. Li (2003), The relationship between the summer precipitation in the Yangtze River valley and the boreal spring Southern Hemisphere

annular mode, Geophysical Research Letters, 30(24), 2266, doi:10.1029/2003GL018381.

Neale, R. B., et al. (2010), NCAR Tech. Note NCAR/TN-486+STR

Nolte, C.G., Gilliland, A.B., Hogrefe, C., Mickley, L.J., 2008. Linking global to regional models to assess future climate impacts on surface ozone levels in the United States. J. Geophys. Res 113, D14307.

Ohara, T., H. Akimoto, J. Kurokawa, N. Horii, K. Yamaji, X. Yan, and T. Hayasaka (2007), An Asian emission inventory of anthropogenic emission sources for the period 1980–2020, Atmos pheric Chemistry and Physics, 7(16), 4419-4444, doi:10.5194/acp-7-4419-2007.

Olivier, J., Van Aardenne, J., Dentener, F., Ganzeveld, L., JAHW, P., 2005. Recent trends in global greenhouse gas emissions: regional trends and spatial distribution of key sources.(169Kb) In:" Non-CO 2 Greenhouse Gases (NCGG-4)", A. van Amstel (coord.). Millpress, Rotterdam, ISBN 90, 043.

Park, R., Kim, S.-W., 2014. Air quality modeling in East Asia: present issues and future directions. Asia-Pacific J Atmos Sci 50, 105-120.

Park, R.J., Jacob, D.J., Field, B.D., Yantosca, R.M., Chin, M., 2004. Natural and transboundary pollution influences on sulfate-nitrate-ammonium aerosols in the United States: implications for policy. J. Geophys. Res. 109.

Pickering, K.E., Wang, Y., Tao, W.K., Price, C., Müller, J.F., 1998. Vertical distributions of lightning NOx for use in regional and global chemical transport models. Journal of Geophysical Research D: Atmospheres 103, 31203-31216.

Pye, H.O.T., Liao, H., Wu, S., Mickley, L.J., Jacob, D.J., Henze, D.K., Seinfeld, J.H., 2009. Effect of changes in climate and emissions on future sulfate-nitrate-ammonium aerosol levels in the United States. Journal of Geophysical Research: Atmospheres 114, D01205.

Racherla, P.N., Adams, P.J., 2008. The response of surface ozone to climate change over the Eastern United States. Atmos. Chem. Phys. 8, 871-885.

Rasmussen, D.J., Fiore, A.M., Naik, V., Horowitz, L.W., McGinnis, S.J., Schultz, M.G., 2012. Surface ozone-temperature relationships in the eastern US: A monthly climatology for evaluating chemistry-climate models. Atmospheric Environment 47, 142-153.

Rayner, N. A., D. E. Parker, E. B. Horton, C. K. Folland, L. V. Alexander, D. P. Rowell, E. C. Kent, and A. Kaplan (2003), Global analyses of sea surface temperature, sea ice, and night marine air temperature since the late nineteenth century, Journal of Geophysical Research D: Atmospheres, 108(14).

Riahi, K., Grübler, A., Nakicenovic, N., 2007. Scenarios of long-term socio-economic and environmental development under climate stabilization. Technological Forecasting and Social Change 74, 887-935.

Riahi, K., Rao, S., Krey, V., Cho, C., Chirkov, V., Fischer, G., Kindermann, G., Nakicenovic, N., Rafaj, P., 2011. RCP 8.5—A scenario of comparatively high greenhouse gas emissions. Climatic Change 109, 33-57.

Shapiro, M.A., 1980. Turbulent Mixing within Tropopause Folds as a Mechanism for the Exchange of Chemical Constituents between the Stratosphere and Troposphere. Journal of the Atmospheric Sciences 37, 994-1004.

Shi, N., and Q. Zhu (1996), An abrupt change in the intensity of the East Asian summer monsoon index and its relationship with temperature and precipitation over East China, International Journal of Climatology, 16(7),

757-764, doi:10.1002/(SICI)1097-0088.

Smith, S.J., Wigley, T.M.L., 2006. Multi-gas forcing stabilization with minicam. Energy Journal 27, 373-391.

Sperber, K. R., H. Annamalai, I. S. Kang, A. Kitoh, A. Moise, A. Turner, B. Wang, and T. Zhou (2013), The Asian summer monsoon: an intercomparison of CMIP5 vs. CMIP3 simulations of the late 20th century, Climate Dynamics, 41(9-10), 2711-2744, doi:10.1007/s00382-012-1607-6.

Sohi, S.P., Krull, E., Lopez-Capel, E., Bol, R., 2010. Chapter 2 - A Review of Biochar and Its Use and Function in Soil, in: Donald, L.S. (Ed.), Advances in Agronomy. Academic Press, pp. 47-82.

Streets, D.G., Bond, T.C., Carmichael, G.R., Fernandes, S.D., Fu, Q., He, D., Klimont, Z., Nelson, S.M., Tsai, N.Y., Wang, M.Q., Woo, J.H., Yarber, K.F., 2003. An inventory of gaseous and primary aerosol emissions in Asia in the year 2000. J. Geophys. Res. 108.

Stubi, R., Levrat, G., 2008. In-flight comparison of Brewer-Mast and electrochemical concentration cell ozonesondes. Journal of Geophysical Research. D. Atmospheres 113.

Szopa, S., Balkanski, Y., Schulz, M., Bekki, S., Cugnet, D., Fortems-Cheiney, A., Turquety, S., Cozic, A., Déandreis, C., Hauglustaine, D., Idelkadi, A., Lathière, J., Lefevre, F., Marchand, M., Vuolo, R., Yan, N., Dufresne, J.L., 2013. Aerosol and ozone changes as forcing for climate evolution between 1850 and 2100. Climate Dynamics 40, 2223-2250.

Tai, A.P.K., Mickley, L.J., Jacob, D.J., 2010. Correlations between fine particulate matter (PM2.5) and meteorological variables in the United States: Implications for the sensitivity of PM2.5 to climate change. Atmospheric Environment 44, 3976-3984.

Tai, A.P.K., Mickley, L.J., Jacob, D.J., 2012a. Impact of 2000–2050 climate change on fine particulate matter (PM2.5) air quality inferred from a multi-model analysis of meteorological modes. Atmos. Chem. Phys. 12, 11329-11337.

Tai, A.P.K., Mickley, L.J., Jacob, D.J., Leibensperger, E.M., Zhang, L., Fisher, J.A., Pye, H.O.T., 2012b. Meteorological modes of variability for fine particulate matter (PM2.5) air quality in the United States: Implications for PM2.5 sensitivity to climate change. Atmospheric Chemistry and Physics 12, 3131-3145.

Taylor, K.E., Stouffer, R.J., Meehl, G.A., 2012. An Overview of CMIP5 and the Experiment Design. Bulletin of the American Meteorological Society 93, 485-498.

Trenberth, K. E., D. P. Stepaniak, and J. M. Caron (2000), The Global Monsoon as Seen through the Divergent Atmospheric Circulation, Journal of Climate, 13(22), 3969-3993, doi:10.1175/1520-0442.

Twomey, S. (1977), The Influence of Pollution on the Shortwave Albedo of Clouds, Journal of the Atmospheric Sciences, 34(7), 1149-1152, doi:10.1175/1520-0469(1977)034<1149:TIOPOT>2.0.CO;2.

Unger, N., Shindell, D.T., Koch, D.M., Amann, M., Cofala, J., Streets, D.G., 2006. Influences of man-made emissions and climate changes on tropospheric ozone, methane, and sulfate at 2030 from a broad range of possible futures. Journal of Geophysical Research: Atmospheres 111, D12313.

Vertenstein, M., Craig, T., Middleton, A., Feddema, D., Fischer, C., 2012. CESM1. 0.4 User's Guide. National Center for Atmospheric Research, Boulder, CO [online]. Available from: http://www. cesm. ucar. edu/models/cesm1. 0/cesm/cesm_doc_1_0_4/book1. html [Accessed 4 May

2012].

Voulgarakis, A., Naik, V., Lamarque, J.F., Shindell, D.T., Young, P.J., Prather, M.J., Wild, O., Field, R.D., Bergmann, D., Cameron-Smith, P., Cionni, I., Collins, W.J., Dalsøren, S.B., Doherty, R.M., Eyring, V., Faluvegi, G., Folberth, G.A., Horowitz, L.W., Josse, B., MacKenzie, I.A., Nagashima, T., Plummer, D.A., Righi, M., Rumbold, S.T., Stevenson, D.S., Strode, S.A., Sudo, K., Szopa, S., Zeng, G., 2013. Analysis of present day and future OH and methane lifetime in the ACCMIP simulations. Atmos. Chem. Phys. 13, 2563-2587.

Vuuren, D., Elzen, M.J., Lucas, P., Eickhout, B., Strengers, B., Ruijven, B., Wonink, S., Houdt, R., 2007. Stabilizing greenhouse gas concentrations at low levels: an assessment of reduction strategies and costs. Climatic Change 81, 119-159.

Wang, B., and Q. Ding (2006), Changes in global monsoon precipitation over the past 56 years, Geophysical Research Letters, 33(6), L06711, doi:10.1029/2005GL025347.

Wang, B., F. Huang, Z. Wu, J. Yang, X. Fu, and K. Kikuchi (2009), Multi-scale climate variability of the South China Sea monsoon: A review, Dynamics of

Atmospheres and Oceans, 47(1–3), 15-37, doi:http://dx.doi.org/10.1016/j.dynatmoce.2008.09.004.

Wang, B., LinHo, Y. Zhang, and M. M. Lu (2004), Definition of South China Sea Monsoon Onset and Commencement of the East Asia Summer Monsoon, Journal of Climate, 17(4), 699-710, doi:10.1175/2932.1.

Wang, B., R. Wu, and K. M. Lau (2001), Interannual Variability of the Asian Summer Monsoon: Contrasts between the Indian and the Western North Pacific–East Asian Monsoons, Journal of Climate, 14(20), 4073-4090, doi:10.1175/1520-0442.

Wang, B., Z. Wu, J. Li, J. Liu, C.-P. Chang, Y. Ding, and G. Wu (2008), How to Measure the Strength of the East Asian Summer Monsoon, Journal of Climate, 21(17), 4449-4463, doi:10.1175/2008JCLI2183.1.

Wang, Y., Jacob, D.J., Logan, J.A., 1998. Global simulation of tropospheric O3-NO x -hydrocarbon chemistry: 3. Origin of tropospheric ozone and effects of nonmethane hydrocarbons. Journal of Geophysical Research: Atmospheres 103, 10757-10767.

Wang, Y., Shen, L., Wu, S., Mickley, L., He, J., Hao, J., 2013. Sensitivity of

surface ozone over China to 2000–2050 global changes of climate and emissions. Atmospheric Environment 75, 374-382.

Webster, M.D., Babiker, M., Mayer, M., Reilly, J.M., Harnisch, J., Hyman, R., Sarofim, M.C., Wang, C., 2002. Uncertainty in emissions projections for climate models. Atmospheric Environment 36, 3659-3670.

Werneth, C.M., Dhar, M., Maung, K.M., Sirola, C., Norbury, J.W., 2010. Numerical Gram-Schmidt orthonormalization. European Journal of Physics 31, 693-700.

Woo, J.-H., Choi, K.-C., Kim, H.K., Baek, B.H., Jang, M., Eum, J.-H., Song, C.H., Ma, Y.-I., Sunwoo, Y., Chang, L.-S., Yoo, S.H., 2012. Development of an anthropogenic emissions processing system for Asia using SMOKE. Atmospheric Environment 58, 5-13.

Wu, S., Mickley, L.J., Jacob, D.J., Logan, J.A., Yantosca, R.M., Rind, D., 2007. Why are there large differences between models in global budgets of tropospheric ozone? Journal of Geophysical Research: Atmospheres 112, D05302.

Wu, S., Mickley, L.J., Jacob, D.J., Rind, D., Streets, D.G., 2008a. Effects of

2000–2050 changes in climate and emissions on global tropospheric ozone and the policy-relevant background surface ozone in the United States. Journal of Geophysical Research 113, 1-12.

Wu, S., Mickley, L.J., Leibensperger, E.M., Jacob, D.J., Rind, D., Streets, D.G., 2008b. Effects of 2000–2050 global change on ozone air quality in the United States. Journal of Geophysical Research: Atmospheres 113, D06302.

Yan, F., Winijkul, E., Streets, D.G., Lu, Z., Bond, T.C., Zhang, Y., 2014. Global emission projections for the transportation sector using dynamic technology modeling. Atmos. Chem. Phys. 14, 5709-5733.

Young, P.J., Archibald, A.T., Bowman, K.W., Lamarque, J.F., Naik, V., Stevenson, D.S., Tilmes, S., Voulgarakis, A., Wild, O., Bergmann, D., Cameron-Smith, P., Cionni, I., Collins, W.J., Dalsøren, S.B., Doherty, R.M., Eyring, V., Faluvegi, G., Horowitz, L.W., Josse, B., Lee, Y.H., MacKenzie, I.A., Nagashima, T., Plummer, D.A., Righi, M., Rumbold, S.T., Skeie, R.B., Shindell, D.T., Strode, S.A., Sudo, K., Szopa, S., Zeng, G., 2013. Pre-industrial to end 21st century projections of tropospheric ozone from the Atmospheric Chemistry and Climate Model Intercomparison Project (ACCMIP). Atmos. Chem. Phys. 13, 2063-2090.

Yu, R., B. Wang, and T. Zhou (2004), Tropospheric cooling and summer monsoon weakening trend over East Asia, Geophysical Research Letters, 31(22), L22212, doi:10.1029/2004GL021270.

Zeng, G., Pyle, J.A., Young, P.J., 2008. Impact of climate change on tropospheric ozone and its global budgets. Atmos. Chem. Phys. 8, 369-387.

Zhang, G.J., McFarlane, N.A., 1995. Sensitivity of climate simulations to the parameterization of cumulus convection in the canadian climate centre general circulation model. Atmosphere - Ocean 33, 407-446.

국문 초록

기후변화와 대기질은 서로에게 긴밀하게 연결되어 있다. 예를 들어 오존이나 에어로졸은 바람이나 온도변화 같은 기후변화에 의하여 농도가 변하게 되며, 대기 중 오염 물질은 복사강제력을 변화시킴으로써 기후에 직접적으로 영향을 미친다. 하지만 기후와 대기질 간의 상호작용에 대한 이해는 아직 부족하다. 본 연구의 목표는 이러한 기후와 대기질 간의 상호작용에 대한 이해를 증진시키고 이를 통해 불확실성을 줄여나가는 것이다. 그 중에서도 본 논문의 구체적 목표는 여러 기후 대기질 인자 중 오존, 에어로졸, 동아시아 여름몬순의 상호작용에 대하여 중점적 알아보았다. 1) 동아시아 에어로졸이 동아시아 여름몬순에 미치는 영향 2) 미래 RCP 시나리오에서의 오존의 변화 3) 동아시아 여름몬순과 동아시아 오존 농도와의 상관관계라는 세 개의 주제를 통하여 연구를 진행하였다. 본 논문에서는 기후모형을 이용하여 인위적인 황산염의 증가가 동아시아 여름몬순에 미치는 영향에 대하여 살펴보았다. SST 의 변화는 최근 몬순의 세기를 약화시키는 주요한 인자였으며 황산염은 이와는 반대로 최근의 수십 년간 동아시아 몬순의 세기를 약하게 강화시키는 것으로 분석되었다. 황산염에 의한 지면 복사 냉각은 극지와 중위도간의 온도 차이를 줄임으로써 제트 꼬리 지역의 제트를 약화시키고 그 결과 이차순환으로 인하여 강수를 감소시키는 것으로 분석되었다. 본 연구에서는 기후모형과 대기화학

수송모형을 이용하여 인위적 활동과 기후변화에 따른 2050 년대의 오존의 변화에 대하여 살펴보았다. 2050 년의 지면오존 농도는 현재에 비하여 RCP6.0, 4.5, 2.6 시나리오에서 각각 −3.3, −3.7, −4.2 ppbv 만큼 차이 나는 것으로 모의되었다. 이에 반해서 RCP8.5 시나리오에서는 2.1 ppbv 만큼 증가하는 경향을 보였다. 지면오존농도의 감소는 NO_x 배출량의 감소로 인하여 주로 감소한 것으로 분석되었다. 기후 변화에 의한 오존의 변화에 대해서도 분석을 진행하였다. 육지에서는 온도 증가에 의하여 최대 2.2 ppbv 의 오존 증가를 야기하였으나 바다에서는 절대습도의 증가로 최대 0.8 ppbv 의 감소를 야기하였다.본 논문에서는 현재와 미래의 동아시아 여름몬순과 동아시아 지면 오존의 상관관계에 대하여도 알아보았다. 동아시아 여름몬순이 강할 때 중국 동해의 순환으로 인하여 중국 내륙에서는 오존의 농도가 증가하고 풍하층에서는 오존의 농도가 감소하는 경향이 보였다. 2050 년대의 몬순변화에 따른 오존의 변화는 2000 년대에 비하여 반대의 상관성을 보였다. 하지만 이와 같은 상반된 관계는 기후변화로 인하여 동아시아의 여름몬순의 정의가 바뀌어 일어난 현상이며 이를 보정하였을 때는 2000 년대와 유사한 경향을 보였다. 하지만 몬순에 의한 2050 년대의 오존의 변화는 2000 년대에 비해서는 크기가 약하게 나타났다.

주요어: 오존, 황산염, 동아시아 여름몬순, 기후변화, 대기화학 수송모형

학번: 2008−20393